NK314 potentiates antitumor activity with adult T-cell leukemia-lymphoma cells by inhibition of dual targets on topoisomerase IIα and DNA-dependent protein kinase

Takashi Hisatomi,[1] Naoko Sueoka-Aragane,[1] Akemi Sato,[1] Rika Tomimasu,[1] Masaru Ide,[1] Akihiro Kurimasa,[2] Kazuya Okamoto,[3] Shinya Kimura,[1] and Eisaburo Sueoka[4]

[1]Department of Internal Medicine, Faculty of Medicine, Saga University, Saga, Japan; [2]Department of Genetic Medicine and Regenerative Therapeutics, Institute of Regenerative Medicine and Biofunction, Graduate School of Medical Science, Tottori University, Tottori Japan; [3]Pharmaceutical Research Laboratories, Nippon Kayaku Co, Ltd, Tokyo, Japan; and [4]Department of Transfusion Medicine, Saga University Hospital, Saga, Japan

Adult T-cell leukemia-lymphoma (ATL) is an aggressive disease, incurable by standard chemotherapy. NK314, a new anticancer agent possessing inhibitory activity specific for topoisomerase IIα (Top2α), inhibited the growth of various ATL cell lines (50% inhibitory concentration: 23-70nM) with more potent activity than that of etoposide. In addition to the induction of DNA double-strand breaks by inhibition of Top2α, NK314 induced degradation of the catalytic subunit of DNA-dependent protein kinase (DNA-PKcs), resulting in impaired DNA double-strand break repair. The contribution of DNA-PK to inhibition of cell growth was affirmed by the following results: NK314 inhibited cell growth of M059J (a DNA-PKcs–deficient cell line) and M059K (a cell line with DNA-PKcs present) with the same potency, whereas etoposide exhibited weak inhibition of cell growth with M059K cells. A DNA-PK specific inhibitor, NU7026, enhanced inhibitory activity of etoposide on M059K as well as on ATL cells. These results suggest that NK314 is a dual inhibitor of Top2α and DNA-PK. Because ATL cells express a high amount of DNA-PKcs, NK314 as a dual molecular targeting anticancer agent is a potential therapeutic tool for treatment of ATL. (*Blood.* 2011;117(13):3575-3584)

Introduction

Adult T-cell leukemia-lymphoma (ATL) is an aggressive and incurable disease caused by type 1 human T-lymphotropic virus (HTLV-1).[1-3] HTLV-1 is a retrovirus endemic to southern Japan and several other countries. After infection, polyclonal expansion of HTLV-1–infected T cells progresses to a state of monoclonal proliferation, with subsequent occurrence of overt ATL after several decades.[2,3] There is presently no cure for ATL; median survival time is only 13 months in advanced ATL, such as acute and lymphoma types.[4,5] Various clinical trials using new therapeutic strategies have been conducted toward improving survival time of patients with aggressive ATL. Among the protocols using combination chemotherapy, VCAP-AMP-VECP therapy consisting of a dose-intensified multiagent chemotherapy improved overall survival with ATL.[4] The protocol included agents overcoming multidrug resistant-related genes, which are frequently expressed in ATL cells.[6,7] Allogeneic hematopoietic stem cell transplantation for young ATL patients is a promising approach, showing an estimated overall 3-year survival of 45%, but the study size was inadequate.[8,9] Treatment with a large dose of zidovudine and interferon-α also produced a good response in patients with acute-type ATL.[10,11]

Recent analyses of molecular mechanisms associated with the occurrence of ATL revealed several molecular targets responsible for cellular transformation and disease progression that could be effective targets for new therapeutic approaches. Based on these studies, targeting therapies for various molecules, such as Tax, NF-κB, Akt/PKB, mTOR, CD25, CD52, and chemokine receptor-4, have been developed under clinical or preclinical investigations using small molecules or monoclonal antibodies.[12-23] The DNA repair system is also a promising target for sensitization of cancer treatment.[24-26] Although genetic instability of proliferating cells is necessary for most cell types to become malignant, cells that are overly unstable genetically will die. Therefore, a treatment that blocks a particular DNA repair system can induce apoptotic cell death of cancer cells but not normal cells. In response to DNA double-strand breaks (DSBs), DNA repair can be mediated by 2 major pathways: homologous recombination and nonhomologous end-joining; more than 90% of DSBs in mammalian cells are repaired by nonhomologous end-joining.[27] Nonhomologous end-joining in mammalian cells is achieved by core protein components, including Ku70/Ku80, DNA-dependent protein kinase (DNA-PK), XRCC4, DNA ligase IV, Artemis, and Cernunnos-XLF.[28,29]

NK314, a synthetic derivative of benzo[c]phenanthridine, is a unique anticancer agent possessing specific and potent inhibitory activity against topoisomerase IIα (Top2α).[30-32] We found that NK314 inhibited ATL cell lines with greater potency than etoposide, a Top2 inhibitor frequently used in practice. Because the range of 50% inhibitory concentration values of NK314 for ATL cell lines and non-ATL cell lines differs from those of etoposide, we investigated other targets of NK314 for induction of apoptosis and inhibition of cell growth of ATL cell lines. In this paper, we demonstrate that NK314 induced degradation of DNA-PKcs and inhibited DNA DSBs repair. The results suggest that NK314 is a new type of anticancer drug possessing inhibitory activity

Submitted February 22, 2010; accepted December 5, 2010. Prepublished online as *Blood* First Edition paper, January 18, 2011; DOI 10.1182/blood-2010-02-270439.

The online version of this article contains a data supplement.

The publication costs of this article were defrayed in part by page charge payment. Therefore, and solely to indicate this fact, this article is hereby marked "advertisement" in accordance with 18 USC section 1734.

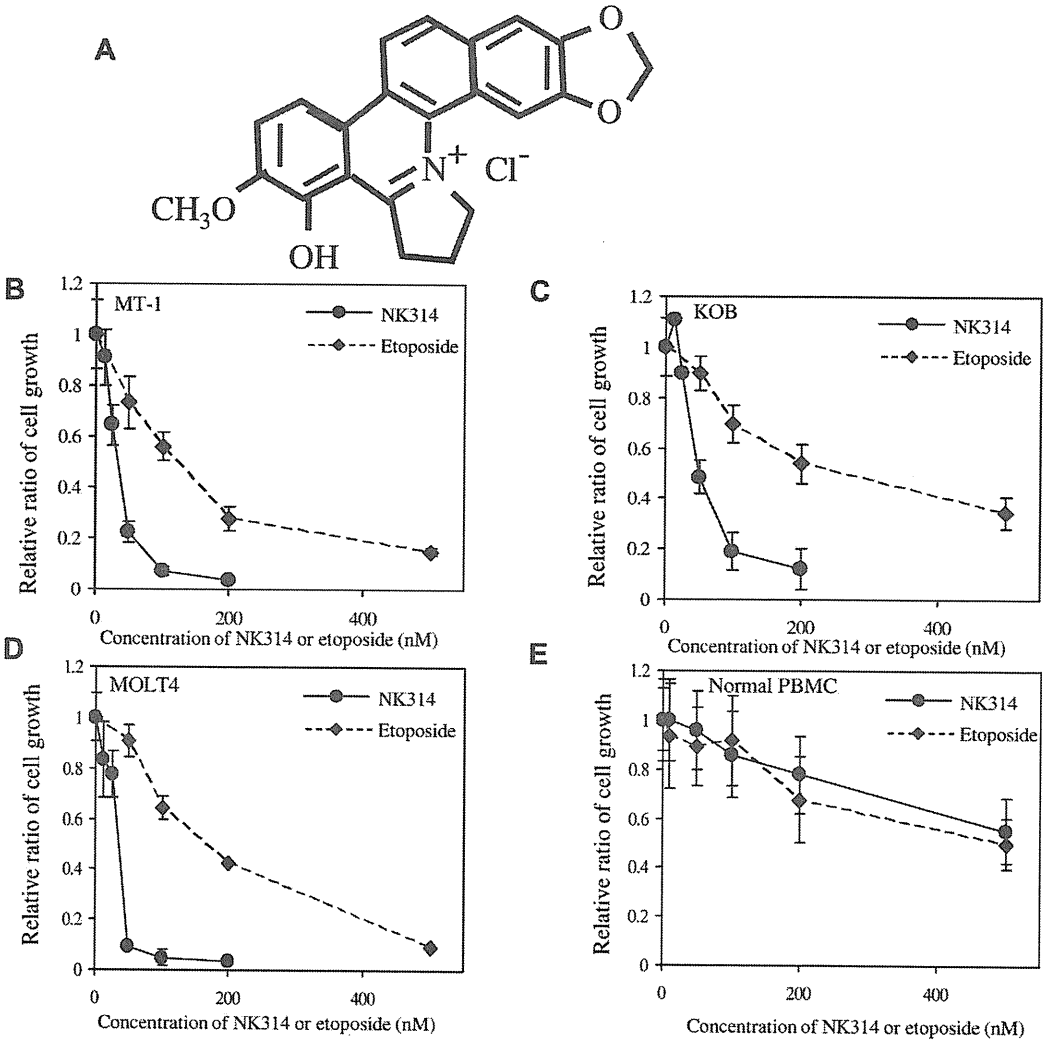

Figure 1. NK314 inhibits cell growth of ATL cell lines. (A) Structure of NK314. (B-E) Inhibition of cell growth of ATL-related cell lines MT-1 (B), KOB (C), MOLT4 (D), and normal PBMCs (E) by treatment with NK314 or etoposide. NK314 (●) or etoposide (♦) were added at various concentrations in culture media, and cell growth rates were determined by trypan blue staining 48 hours after treatment. The relative ratio of cell growth is shown; values are mean ± SD of triplicate analyses.

against Top2α and DNA-PK, and so is a promising candidate for treatment of ATL.

Methods

Chemicals and antibodies

NK314 (Figure 1A) was synthesized at Nippon Kayaku and dissolved in distilled water before use.[30-32] Etoposide was also synthesized at Nippon Kayaku. NU7026 was purchased from Sigma-Aldrich. Sources of antibodies were as follows: PARP-1, Ku70, and actin (Santa Cruz Biotechnology) and DNA-PKcs and Ku86 (Lab Vision Corporation).

Cell lines and culture conditions

The study protocol was approved by the Clinical Research Ethics Committee of Saga University; and when applicable, informed consent was obtained in compliance with the Declaration of Helsinki. Eight ATL cell lines were used: 6 ATL-derived cell lines and 2 HTLV-1–infected T-cell lines. ATN-1, KK1, ST1, and KOB were established from ATL patients and kindly provided by Dr Yasuaki Yamada of Nagasaki University Graduate School of Biomedical Sciences; the patient origins of these cells were confirmed by concordance of the integration sites of HTLV-1 proviral DNA and/or rearrangement profiles of the T-cell receptor β-chain gene.[33-35] MT-1 was derived form a patient with ATL.[36] MT-2 was established by cocultivation of human cord blood lymphocytes from a normal subject with peripheral blood mononuclear cells (PBMCs) from an ATL patient.[37] OMT is an HTLV-1–infected T-cell line.[38] MT-2 was kindly provided by Dr Kunitada Shimotono of Kyoto University, Japan. MOLT-4, Jurkat, M059J, and M059K cells were purchased from ATCC. Stable transformants with DNA-PK cDNA (MJ L24) or vector alone (MJ NA) introduced into M059J cells were established as described previously.[39] MT-1, MT-2, ATN-1, MOLT-4, and Jurkat cells were cultured in RPMI 1640 containing 10% fetal bovine serum (FBS). M059K, M059J, MJ L24, and MJ NA glioblastoma cell lines were cultured in F-12/Dulbecco modified Eagle medium supplemented with 10% FBS, 1% penicillin/streptomycin, and 1% nonessential amino acids. OMT, KOB, KK1, and ST1 were interleukin-2 (IL-2) dependent and were cultured in RPMI 1640 containing 10% FBS with 10 ng/mL recombinant human IL-2, kindly provided by Takeda Chemical Industries. Normal PBMCs were collected from 5 healthy volunteers and cultured in RPMI 1640 containing 10% FBS.

Analysis of cell proliferation, cell cycle, and apoptosis

ATL, MOLT-4, and Jurkat cells (2×10^6 cells) were cultured in a 10-mL culture bottle for 1 hour and treated with the indicated concentrations of NK314 and etoposide, with or without the DNA-PK inhibitor NU7026 for

48 hours. The number of cells was determined with trypan blue staining or Cell Counting Kit-8 (Dojindo Molecular Technologies). Relative ratio of cell growth, calculated by dividing by the number of untreated cells, is shown as mean plus or minus SD of triplicate analyses. Cell-cycle analysis of ATL cells was performed using flow cytometry. Cells (1×10^6 cells) were treated with the indicated concentrations of NK314. Twenty-four hours after treatment, cells were collected and fixed with 2% paraformaldehyde followed by 70% ethanol. Cells were treated with RNase A (0.25 mg/mL) at 37°C for 30 minutes and stained with 50 μg/mL of propidium iodide (BD Biosciences). Cellular DNA content was analyzed using flow cytometry, and cell-cycle profiles were determined with CellQuest software Version 3.1 (BD Biosciences). Analysis of apoptosis was conducted using a MEBCYTO Apoptosis Kit (Medical & Biologic Laboratories). Cells treated with NK314 for 24 hours were simultaneously stained with annexin V–fluorescein isothiocyanate and propidium iodide according to the manufacturer's instructions. Stained cells were subjected to fluorescence-activated cell sorter analysis to determine the number of apoptotic cells. Induction of apoptosis was also assessed by degradation of PARP-1. Cell extracts were obtained after treatment with NK314 or etoposide at each time point, and the degradation of PARP-1 was determined by Western blot analysis.

Western blot analysis

Whole cell lysates of ATN-1,MT-1, and OMT cells were prepared from cells using lysis buffer containing 50mM Tris-HCl at pH 8.0, 150mM NaCl, 5mM $MgCl_2$, 1% Triton X-100, 0.1% sodium dodecyl sulfate, 0.5% sodium deoxycholate, 40mM sodium fluoride, 1mM sodium orthovanadate, 1 μg/mL leupeptin, 10 μg/mL aprotinin, and 1mM phenylmethylsulfonyl fluoride, as reported previously.[40] Protein was separated using a 10% NuPAGE electrophoresis system (Novex), transferred to a nitrocellulose membrane (Schleicher & Schuell), blocked with 5% milk at 4°C overnight, and finally reacted with primary antibodies. An enhanced chemiluminescence kit (GE Healthcare) was used for detection.

γH2AX measurement using flow cytometry, and irradiation

After treatment with the indicated concentration of NK314 for 1, 6, 24, or 48 hours, cells were harvested and washed with phosphate-buffered saline 3 times. γH2AX was detected using an H2AX Phosphorylation Assay Kit (Millipore). Cells were treated with RNase A (10 μg/mL) at 37°C for 30 minutes and counterstained with propidium iodide (25 μg/mL). Stained samples were analyzed using flow cytometry (BD Biosciences).

DNA repair capacity of NK314 after irradiation was evaluated as follows. After treatment with NK314 for 1 hour, cells were irradiated at 4 Gy, followed by detection of γH2AX using flow cytometry at the indicated period. Cells were irradiated using an IBL437C-I ^{137}Cs γ-irradiator (CIS Bio International) at 3.5 Gy/min. DNA repair capacity was presented as time courses of γH2AX induction and relative ratios of $\gamma H2AX^+$ cells 5 minutes and 2 hours after γ-irradiation combined with compounds compared with γ-irradiation alone.

Colony-forming assay

Colony-forming assay was performed using MethoCult Express (Stem Cell Technologies). Whole bone marrow cells from a healthy volunteer were diluted with Iscove modified Dulbecco medium (Invitrogen) plus 2% FBS (Nichirei Corporation), and added to MethoCult Express. The cells were dispensed into 35-mL culture dishes at a final concentration of 1.5×10^4 cells/mL/dish. After culture at 37°C in 5% CO_2 with more than or equal to 95% humidity for 7 days, all colonies containing more than 20 cells were counted.

Animal experiments

Animal experiments were approved by the Animal Research Ethics Committee of Saga University. MT-1 cells (5×10^5) were injected into the dorsal flanks of SCID mice (C.B-17/IcrCrj-*scid/scid*, Charles River Laboratories) after 4 Gy irradiation. A total of 10 or 20 mg/kg of NK314 or phosphate-buffered saline was injected intraperitoneally at days 14, 28, and 42 after inoculation. Tumor volumes, defined as $(\text{short axis})^2 \times (\text{long axis})/2$, were measured every 3 days and are expressed as mean plus or minus SD. Cell count in peripheral blood was obtained with a K-4500 auto blood cell counter (Sysmex Corporation). Biochemical analysis was performed by SRL.

Table 1. Growth inhibition of ATL cell lines induced by NK314 or etoposide

Cell line	$IC_{50, nM}$ NK314	Etoposide
IL-2–independent		
ATN-1	38.3	135.8
MT-1	34.8	115.0
ST1	45.2	138.0
MT-2	22.6	76.7
IL-2–dependent		
KOB	58.2	248.6
ST1 (IL-2)	71.3	214.5
KK1	60.1	194.2
OMT	51.3	344.7
MOLT4	32.6	157.9
Jurkat	29.2	145.8
Normal PBMCs	≥ 500	≥ 500

Statistical analysis

Tumor volumes were compared using a 2-sided *t* test. Statistical analyses were conducted using SPSS Version 11.0J (SPSS Japan).

Results

NK314 inhibited cell growth and induced apoptosis via G_2/M arrest of ATL-related cell lines

NK314 is a synthetic benzo[c]phenanthridine alkaloid that shows strong inhibitory activity against Top2α and antitumor activity.[30-32] Because NK314 inhibits Top2α more specifically and more potently than etoposide, which is a key drug for ATL treatment, we investigated the antitumor activity of NK314 in ATL cells. Various ATL-related (6 ATL-derived cell lines and 2 HTLV-1–infected) T-cell lines were cultured with or without IL-2. Non-ATL T-cell leukemia cell lines, MOLT4, and Jurkat cells were also used in this study. NK314 or etoposide was added at various concentrations in culture media, and cell growth rates were determined with trypan blue staining 48 hours after treatment. NK314 inhibited cell growth of ATL cell lines in a dose-dependent manner. Representative results using an IL-2–independent cell line, MT-1, and an IL-2–dependent cell line, KOB, are shown in Figure 1B-C. The 50% inhibitory concentration values of NK314 and etoposide ranged from 22.6 to 71.3nM and 76.7 to 344.7nM, respectively (Table 1). Non-ATL cell lines, such as MOLT4 and Jurkat cells, were also more sensitive to NK314 than to etoposide. Inhibitory effects of cell growth by these compounds were weak on normal PBMCs. To examine the mechanisms of growth inhibition by NK314, we next investigated the effects of NK314 on the cell cycle and on induction of apoptosis in ATL cell lines and PBMCs. NK314 induced G_2/M arrest dose-dependently on all cell lines examined, except PBMCs, which were kept in G_0/G_1 phase (Figure 2A). Etoposide also induced G_2/M arrest on all cell lines examined (data not shown). Induction of G_2/M arrest was associated with apoptosis analyzed by induction of annexin V and cleavage of PARP-1, although the activities of NK314 for induction of apoptosis on ATL cell lines

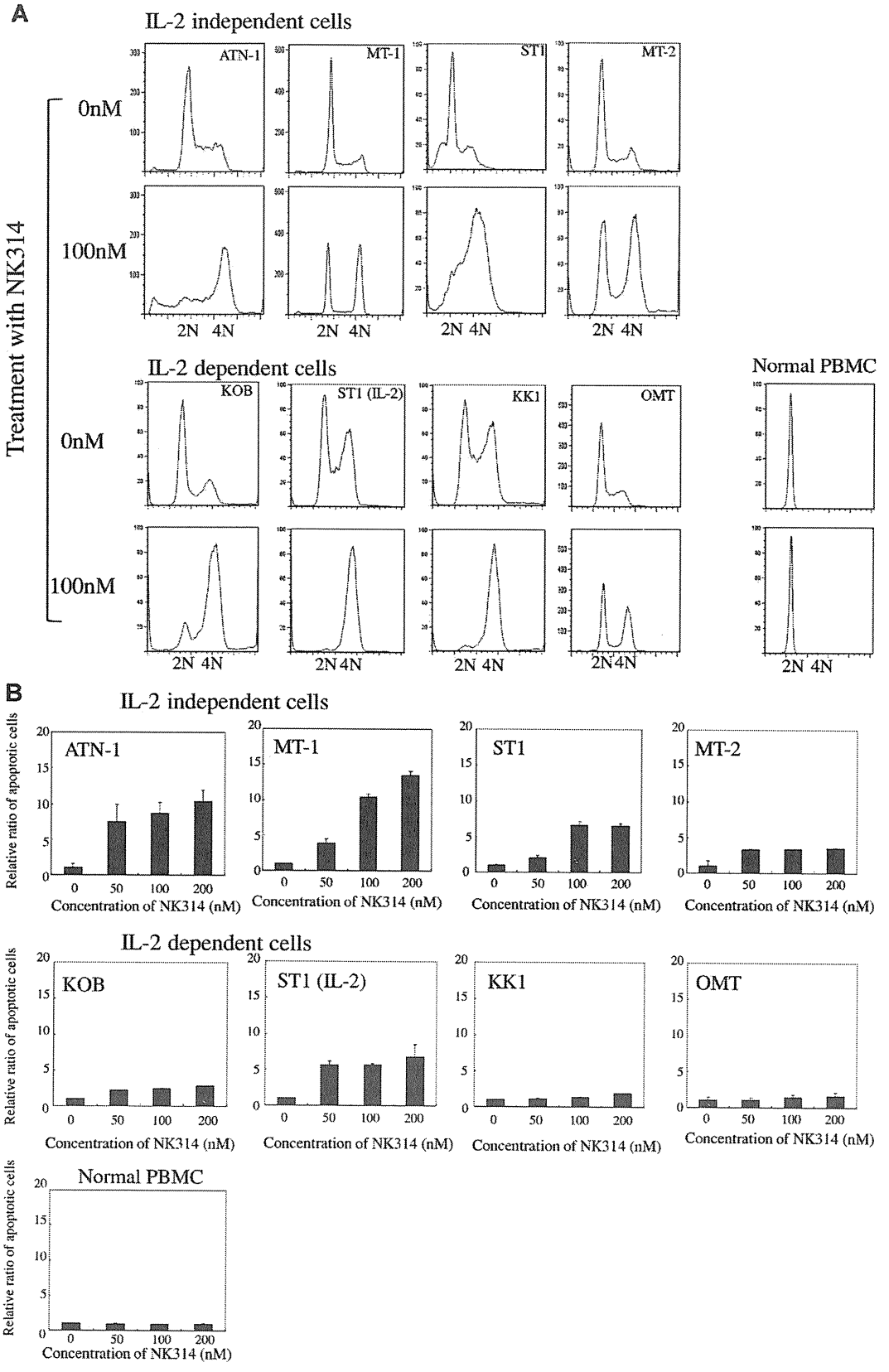

Figure 2. Effect of NK314 on cell cycle and apoptosis in ATL cell lines. (A) Cell-cycle analysis using flow cytometry after NK314 treatment of ATL cells. ATL cells were treated with the indicated concentrations of NK314 and then fixed and stained with propidium iodide 24 hours after treatment. Cellular DNA content and cell cycle profiles were determined with CellQuest software Version 3.1 (BD Biosciences). (B) Annexin V and propidium iodide analysis of ATL cells treated with NK314. Cells treated with NK-314 for 24 hours were simultaneously stained with annexin V and propidium iodide according to the manufacturer's instructions. Stained cells were conducted to a fluorescence-activated cell sorter analysis to determine the number of apoptotic cells. The ratio of apoptotic cells was calculated as number of apoptotic cells treated with NK314 of the indicated concentrations divided by the number of untreated cells and expressed as mean ± SD of triplicate analyses.

varied (Figure 2B; supplemental Data, available on the *Blood* Web site; see the Supplemental Materials link at the top of the online article). Among the cell lines, IL-2–independent cell lines, such as ATN-1 and MT-1, showed stronger induction of apoptosis compared with IL-2–dependent cell lines after treatment with NK314. Because various Top2 inhibitors have been reported to be inducers of G_2/M arrest in cancer cell lines,[41] it is possible that Top2 inhibition was achieved in the ATL cell lines, including IL-2–dependent cell lines, but that the activation of apoptotic pathway was relatively weak in these cell lines. NK314 did not evidence induction of annexin V or cleavage of PARP-1 on PBMCs.

NK314 inhibited repair of DNA DSBs induced by ionizing radiation in ATL cell lines

It has been reported that the inhibition of Top2α induces DNA DSBs, and recent papers suggest that inhibition of DNA damage response can overcome the drug resistance seen in cancer chemotherapy.[24-26] We investigated the effects of NK314 on DNA damage response with or without irradiation. ATL cell lines and PBMCs were treated with NK314 with or without 4 Gy irradiation 1 hour after seeding. The induction of γH2AX was monitored by flow cytometry as a marker of DNA DSBs. In MT-1 cells, NK314 alone gradually increased the number of $\gamma H2AX^+$ cells 24 hours after treatment with apparently stronger potency than that of etoposide, and other IL-2–independent cell lines showed similar tendencies, except MT-2 cells (Figure 3A). However, induction of $\gamma H2AX^+$ cells by NK314 was weak in IL-2–dependent cell lines. These results were comparable with those of apoptosis. Among 8 cell lines examined, induction of DNA damage was more apparent and prolonged by treatment with NK314 compared with etoposide in 7 cell lines. Again, neither NK314 nor etoposide evidenced DNA damage in normal PBMCs. Combining NK314 or etoposide with 4 Gy irradiation induced remarkable induction of $\gamma H2AX^+$ cells 5 minutes after irradiation (supplemental Data). However, disappearance (indicating DNA damage repair) of the positive cells was apparently inhibited after treatment with NK314 in 4 of 8 cell lines examined (supplemental Data). We assessed the effects of these compounds on induction of DNA damage ($\gamma H2AX^+$ cells at 5 minutes) and impairment of DNA repair ($\gamma H2AX^+$ cells at 2 hours; Figure 3B). The induction pattern of $\gamma H2AX^+$ foci 5 minutes after irradiation was comparatively higher in cells treated with NK314, and the population of $\gamma H2AX^+$ foci was apparently larger with NK314 treatment compared with etoposide, especially in IL-2–independent cell lines. These results suggest that NK314 contributes to impairment of DNA repair as well as induction of DNA damage.

DNA-PKcs overexpressed in ATL cells, and NK314 induced protein degradation of DNA-PKcs

DNA-PK is a family of phosphoinositide 3-kinases and a major molecule involved in the repair of DNA DSBs after irradiation and genotoxic stimuli. We determined the amount of DNA-PK complex in ATL cell lines (Figure 4A). The DNA-PK complex consists of Ku86, Ku70, and DNA-PKcs. Expression of Ku proteins is ubiquitous, but DNA-PKcs levels were apparently high in all ATL cell lines compared with normal $CD4^+$ T cells. NK314 induced degradation of DNA-PKcs in 5 of 8 cell lines but did not in OMT cells (Figure 4B). In the case of ST-1 (IL-2–independent) cells, protein fragmentation was not observed, but the amount of DNA-PKcs protein apparently decreased after treatment with NK314. After treatment with etoposide, the degradation of DNA-PKcs was not observed, except in ATN-1 cells; indeed, the amount increased in some cell lines (MT-1, IL-2–independent ST-1, and OMT cells). Ku86 and Ku70 were not altered by treatment with NK314 or etoposide in any ATL cell lines or normal PBMCs (supplemental Data). To clarify the contribution of DNA-PK to the effects of NK314, such as DNA damage response and cell growth inhibition, ATL cell lines were treated with the DNA-PK inhibitor NU7026 in combination with NK314 or etoposide. A total of 10μM of NU7026 alone did not inhibit growth of ATL cells (data not shown). Figure 4C showed combination effects of NU7026 with NK314 or etoposide on cell growth inhibition of ATL cell lines. In combination with etoposide, NU7026 enhanced cell growth inhibition compared with etoposide alone in all 8 cell lines, especially at lower doses. However, in combination with NK314, NU7026 showed enhancement of cell growth inhibition effects on some cell lines, but the effects were marginal (Figure 4C).

Next, we compared the effects of NK314 in a DNA-PKcs–deficient cell line and a parental cell line. The DNA-PK mutant glioblastoma cell line, M059J, did not express any DNA-PKcs (Figure 5A). Parental M059K cells expressed all subunits of DNA-PK complex and were used as a control. Both NK314 and etoposide inhibited cell growth of M059J with almost the same potency, but the effect of etoposide was remarkably weaker on M059K cells, having intact DNA-PKcs than that of NK314 (Figure 5B-C). These results suggest that DNA-PK is involved in sensitivity to cell toxicity induced by these Top2 inhibitors. Together with the results of induction of $\gamma H2AX^+$ cells, it suggests that NK314 possesses both Top2 inhibition (induction of DNA damage) and inhibition of DNA-PK activity (inhibition of DNA repair), resulting in potent cytotoxic effects on ATL cells. To examine this hypothesis, we studied the effect of NU7026 on M059J and M059K cells. Again, NU7026 alone showed no apparent cytotoxic effect on either M059J or M059K (data not shown). In combination with NU7026 and etoposide, NU7026 enhanced the inhibitory activity of etoposide against M059K cells (DNA-PKcs intact), but it did not against M059J cells (DNA-PK deficient) (Figure 5B-C). The additional effect of NU7026 in combination with NK314 was not prominent in either M059K or M059J. To confirm the contribution of DNA-PK to cell growth inhibition of M059 cells by NK314, we introduced DNA-PKcs cDNA into M059J cells (DNA-PKcs–deficient cell line) and established cell lines as reported previously.[39] Among them, we used MJ L24 (DNA-PKcs cDNA introduced) and MJ NA (mock vector introduced) cells in this experiment. Expression of DNA-PKcs and Ku proteins in MJ L24 cells was confirmed by Western blotting (Figure 5A). The growth inhibitory activity of NK314 or etoposide on DNA-PK–deficient MJ NA cells was almost equal to parental M059J cells (Figure 5E). However, cell toxicity of etoposide in MJ L24 cells became weaker, and the effect was comparable with that of DNA-PKcs–intact M059K cells (Figure 5D). Furthermore, NU7026 enhanced cell toxicity in combination with etoposide in MJ L24 cells as shown on M059K cells (Figure 5D). These data clearly show that DNA-PK inhibition contributed to cell growth inhibition of M059 cells, and NK314 inhibits DNA-PK in addition to TopIIα.

NK314 inhibited the tumor growth of MT-1 cells transplanted into SCID mice

To examine the antitumor effects of NK314 against ATL cells in vivo, we established a mouse model carrying a xenograft tumor of ATL cells. Among several cell lines examined, MT-1 cells were stably transplantable to the subcutaneous tissue of SCID mice, so we used this model to evaluate antitumor activity of NK314 against

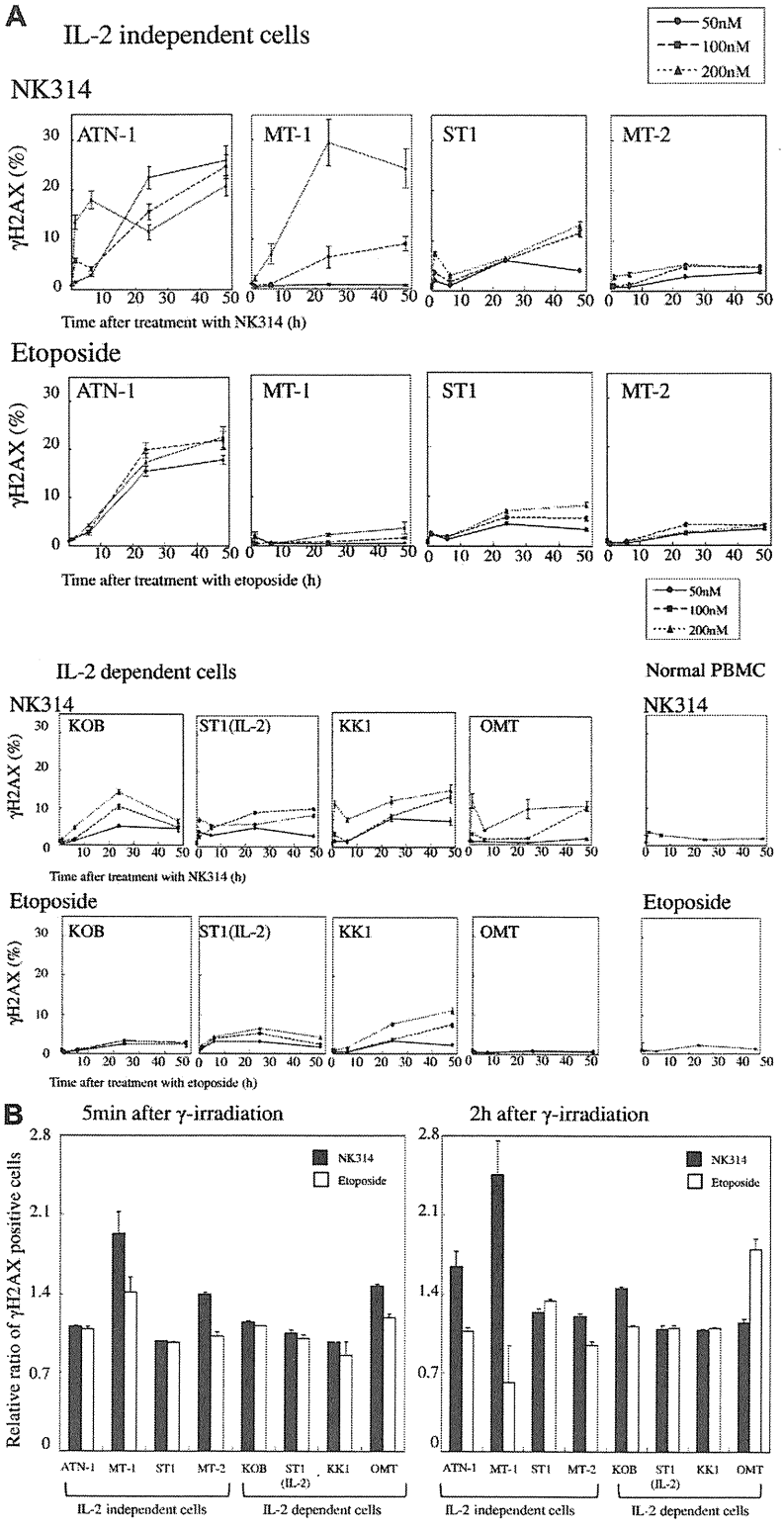

Figure 3. Induction of DNA DSB in ATL cells by NK314 or etoposide and comparison of DNA repair capacity in NK314- or etoposide-treated cells after irradiation. (A) After treatment with the indicated concentrations of NK-314 or etoposide, induction of γH2AX$^+$ foci was determined by flow cytometry using an H2A.X Phosphorylation Assay Kit. The percentage of γH2AX$^+$ foci was calculated by dividing by the number of cells without treatment by the compounds. (B) DNA damage induced by combination treatment with irradiation and the compounds at a dose of 200nM was determined by induction of γH2AX$^+$ foci. DNA damage is expressed as relative ratios of number of γH2AX$^+$ cells at time points of 5 minutes and 2 hours after treatment divided by that of γH2AX$^+$ cells without treatment by the compounds at each time point.

ATL. After 4 Gy irradiation, MT-1 cells were inoculated into subcutaneous tissue of the mouse's back; and 14 days after inoculation, a visible tumor appeared. After that, NK314 was injected intraperitoneally once every 14 days. Figure 6 shows tumor growth curves for the MT-1 cells inoculated in the backs of the mice. We applied several experimental protocols using various NK314 doses and treatment schedules. Because treatment with more than 50 mg/kg of NK314 biweekly showed toxic effects, we used 2 doses (10 and 20 mg/kg) of NK314 biweekly. At a dose of 10 mg/kg, NK314 effectively inhibited tumor growth of MT-1 cells; and apparent side effects, such as body weight loss, myelosuppression, liver dysfunction, or renal insufficiency, were not observed (supplemental Data). We also studied the toxic effects of NK314 using colony-formation assay with normal human bone marrow cells. NK314 dose-dependently inhibited the colony formation of normal human bone marrow cells, but the inhibitory

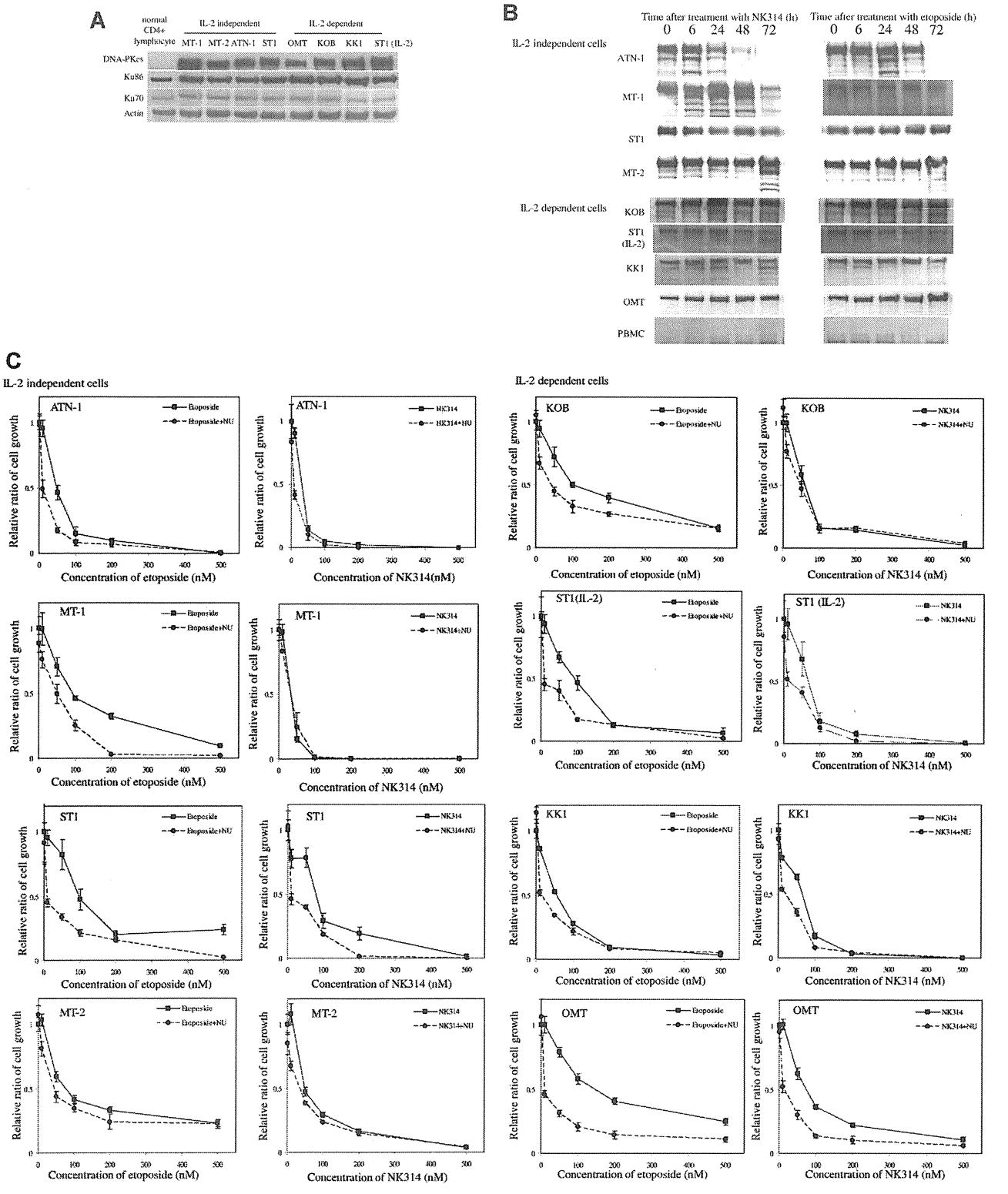

Figure 4. Degradation of DNA-PKcs induced by NK314 in ATL cells. (A) Expression of DNA-PK complex in various ATL cell lines and normal CD4$^+$ lymphocytes was detected using Western blot analysis. The results with normal CD4$^+$ cells were obtained from a different gel in the same experiments with the others. Vertical line(s) have been inserted to indicate a repositioned gel lane. (B) Degradation of DNA-PKcs was determined after treatment with NK314 or etoposide at each time point using Western blot analysis. (C) Contribution of DNA-PK to the inhibition of cell growth by NK314 in ATL cell lines. Cells were treated with etoposide or NK314 with or without NU7026 (NU), a DNA-PK inhibitor. Number of cells was determined with Cell Counting Kit-8. Relative ratio of cell growth was calculated by dividing by the number of untreated cells and expressed as mean ± SD of triplicate analyses.

activity was comparable with, or slightly weaker than, that of etoposide (supplemental Data). These results suggest that biweekly treatment with NK314 at a dose of 10 mg/kg is efficient to inhibit growth of established ATL-cell tumors.

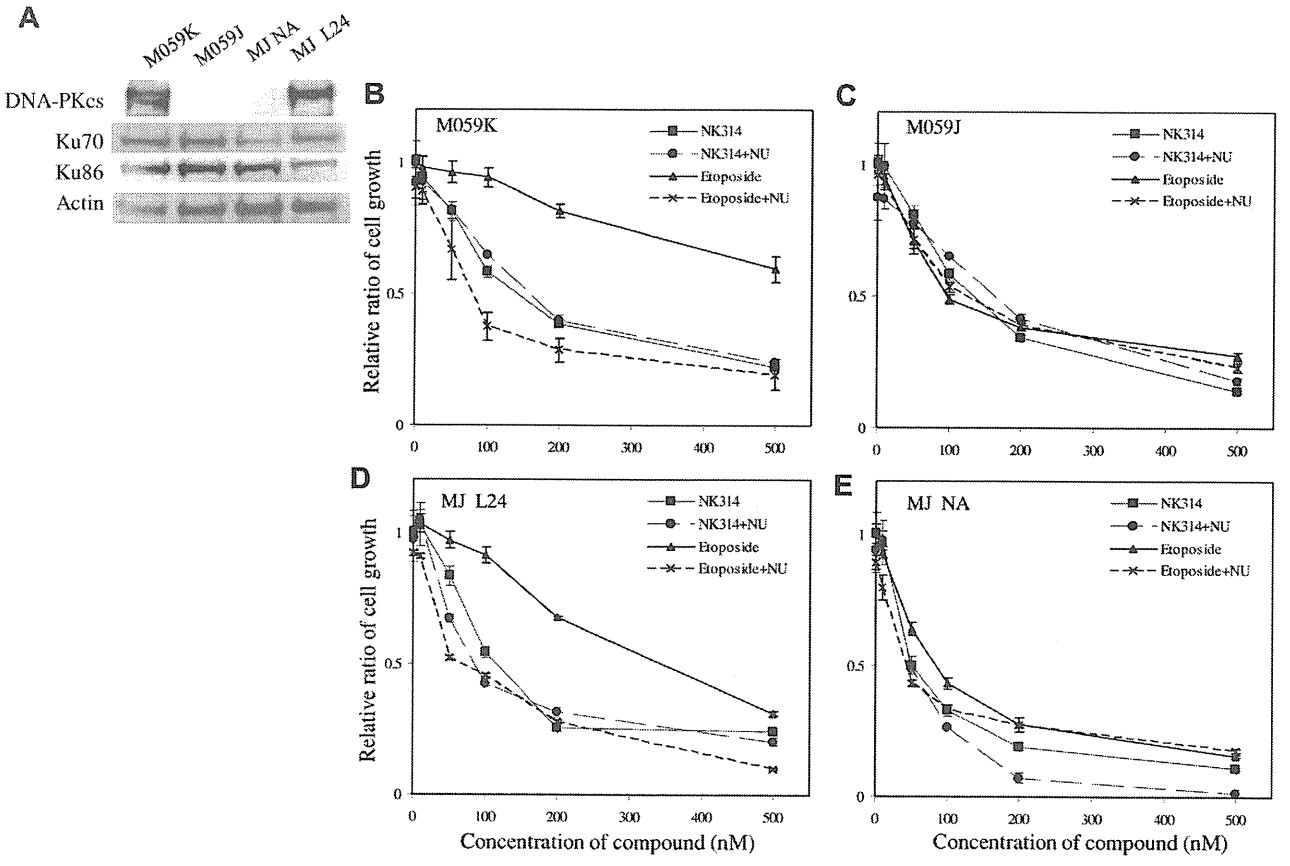

Figure 5. Effect of NK314 on growth of M059 cell lines. (A) Expression of DNA-PK complex in M059K, M059J (a DNA-PKcs mutant), MJ NA (mock vector-transfected), and MJ L24 (DNA-PK cDNA-transfected) cells was detected by Western blot analysis. M059 cells were treated with etoposide or NK314 in combination with or without NU7026 (NU). Effects of NK314 or etoposide on cell growth of M059K (B), M059J (C), MJ L24 (D), or MJ NA (E) were determined with Cell Counting Kit-8. Relative ratio of cell growth was calculated by dividing by the number of untreated cells and expressed as mean ± SD of triplicate analyses.

Discussion

Molecular targeting therapy is a sophisticated treatment strategy for some cancer types, including chronic myeloid leukemia, multiple myeloma, and lung cancer. In the case of ATL, several molecular targets associated with cellular transformation and disease progression have been identified that could be excellent targets for therapy. However, ATL cells display a variety of heterogeneous genetic alterations. It has been suggested that this complexity of genetic changes in ATL cells allows them to easily adapt to a single agent. Even though various combination chemotherapies using multiple anticancer drugs have been applied to the treatment of ATL, they have failed in that the median survival time is limited to only 13 months with the VCAP-AMP-VECP protocol.[4] Therefore, we focused on investigating sensitization toward anticancer drugs or irradiation.

NK314, a new Top2α specific inhibitor, showed potent antitumor activity for ATL with in vitro and in vivo models. In addition to inhibition of Top2α, we found that NK314 inhibited DNA DSB repair mediated by inducing degradation of DNA-PKcs. DNA-PK is a member of the phosphoinositide 3-kinase family and a critical kinase for repair of DNA DSBs initiated with various genotoxic stresses, such as ionizing radiation, oxyradicals, and anticancer agents.[27-29] Various agents for inhibiting DNA-PK have been identified and clinical trials have been conducted using both subclinical and clinical approaches.[42-47] As for ATL cells, it was reported that transcription factor Tax binds to DNA-PKcs and activates DNA-PK. However, the Tax-DNA-PK complex was incapable of repairing new DNA DSBs induced by genotoxic stimuli in ATL cells.[48,49] Considering these results, impairment of DNA-PK mediated DNA DSB repair could be associated with genetic instability and cell transformation in the Tax-dependent early stage of ATL, whereas overexpression of DNA-PK or elevated DNA-PK activity could be associated with multidrug-resistant phenotypes in overt ATL, as reported in other types of cancers.[42-47] In our experiments, it was difficult to analyze the association of Tax expression and effect of NK314 or DNA-PK inhibitor on cell growth inhibition in ATL cells because only one cell line (MT-2) expressed a detectable amount of Tax protein (data not shown). Genetic instability is usually correlated with cell proliferation capacity, and many cancer cell types have a tendency to be genetically unstable. Therefore, impairment of DNA repair capacity in rapidly proliferating cancer cells may induce accumulation of lethal genetic changes, resulting in apoptosis. Indeed, various inhibitors of the DNA repair system can sensitize toward chemotherapy and radiation therapy; their anticancer effects have been investigated in the laboratory and in the subclinical situation.[42-47]

In this paper, we presented evidence that ATL cells express high amounts of DNA-PKcs, and a specific inhibitor of DNA-PK enhanced cell toxicity induced by etoposide. The results prompted us to use DNA-PK inhibitors in combination with anticancer drugs for treatment of ATL. However, the combination therapy poses

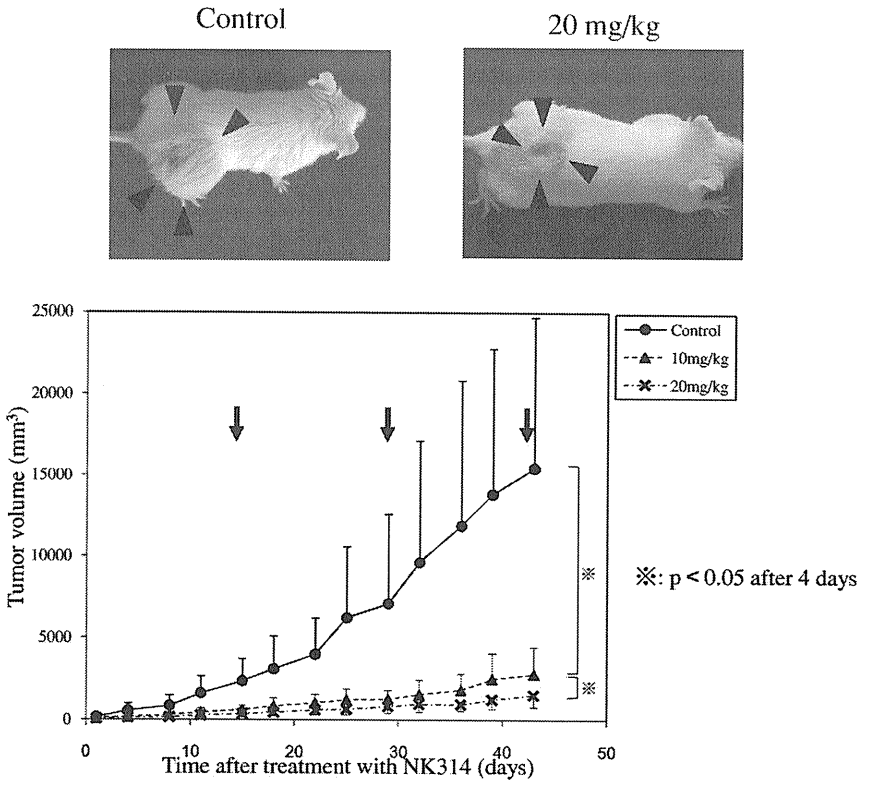

Figure 6. Effect of NK314 on tumor growth of MT-1 cells transplanted into SCID mice. MT-1 cells were injected into the dorsal flank of SCID mice after 4 Gy irradiation. NK-314 at a dose of 10 mg/kg (▲) or 20 mg/kg (×), or phosphate-buffered saline (●), was injected intraperitoneally at days 14, 28, and 42 after inoculation (arrows). Tumor volume was calculated as (short axis)^2 × (long axis)/2.

other problems to be solved, such as bioavailability and side effects of each compound, as well as their interplay. Because NK314 functions dually as a potent inhibitor of Top2α and DNA-PK, monitoring of the aforementioned drug-drug interaction is not necessary. Another problem concerning use of a DNA-PK inhibitor is the occurrence of a second, therapy-related malignancy, such as leukemia or myelodysplastic syndrome, especially in combination with Top2 inhibitors, alkylating agents, and irradiation.[50,51] In the literature, Top2α is more abundantly expressed in cancer cells and regulates the cell cycle.[41,52] Inhibition of Top2α is responsible for cytotoxic effects on cancer cells, whereas inhibition of Top2β might influence the development of a second malignancy. These results suggest that NK314 has an advantage as a new type of anticancer agent in ATL treatment. On the other hand, the DNA-PK inhibitor NU7026 enhanced cytotoxicity of etoposide on ATL cells, but its effects varied among ATL cell lines and the combination effects of NU7026 for etoposide were slightly weaker on IL-2–dependent ATL cell lines than those on IL-2–independent cell lines. Although we have not clarified the mechanisms yet, it is possible that the IL-2 receptor signal activates the phosphoinositide 3 AKT kinase pathway in regulatory T cells, possible counterparts of ATL cells,[53]; thus, treatment with IL-2 on ATL cell lines might act as an antagonistic against a DNA-PK inhibitor.

As for the toxicity of the compounds, we monitored body weight change, myelosuppression, and hepatorenal toxicity in the in vivo experiment involving xenograft tumors. As shown in the supplemental Data, biweekly administration of a dose of 20 mg/kg NK314 showed no apparent hepatorenal toxicity and produced only moderate reduction of leukocytes (not statistically significant). We also investigated the toxicity of NK314 on in vitro cultured human bone marrow cells. The 50% inhibitory concentration of NK314 for colony formation of freshly isolated human bone marrow cells was approximately 100nM, which is comparable with etoposide. Because NK314 has more potent activity for cell growth inhibition of ATL cells, it offers promise for clinical application in the treatment of patients with aggressive ATL.

Acknowledgments

The authors thank Dr Kunitaka Shimotono at Kyoto University for his generous gift of the MT-2 cell line and Takeda Chemical Industries for providing the IL-2.

This work was supported by the Ministry of Education, Culture, Sports, Science and Technology and the Smoking Research Foundation.

Authorship

Contribution: T.H., A.S., R.T. M.I., N.S.-A., and E.S. performed the research and analyzed the data; N.S.-A. edited the paper; R.T., M.I., A.K., and S.K. provided the samples and related data; K.O. provided agents and fruitful discussion; and E.S. designed the research, analyzed the data, and wrote the paper.

Conflict-of-interest disclosure: The authors declare no competing financial interests.

Correspondence: Eisaburo Sueoka, Department of Transfusion Medicine, Saga University Hospital, Saga, 849-8501, Japan; e-mail: sueokae@cc.saga-u.ac.jp.

References

1. Hinuma Y, Nagata K, Hanaoka M, et al. Adult T-cell leukemia: antigen in an ATL cell line and detection of antibodies to the antigen in human sera. *Proc Natl Acad Sci U S A.* 1981;78(10): 6476-6480.
2. Poiesz BJ, Ruscetti FW, Gazdar AF, et al. Detection and isolation of type C retrovirus particles from fresh and cultured lymphocytes of a patient with cutaneous T-cell lymphoma. *Proc Natl Acad Sci U S A.* 1980;77(12):7415-7419.
3. Matsuoka M, Jeang KT. Human T-cell leukaemia virus type 1 (HTLV-1) infectivity and cellular transformation. *Nat Rev Cancer.* 2007;7(4):270-280.
4. Tsukasaki K, Utsunomiya A, Fukuda H, et al. VCAP-AMP-VECP compared with biweekly CHOP for adult T-cell leukemia-lymphoma. *J Clin Oncol.* 2007;25(34):5458-5464.
5. Yamada Y, Tomonaga M, Fukuda H, et al. A new G-CSF-supported combination chemotherapy, LSG15, for adult T-cell leukaemia-lymphoma: Japan Clinical Oncology Group Study 9303. *Br J Haematol.* 2001;113(2):375-382.
6. Lau A, Nightingale S, Taylor GP, et al. Enhanced MDR1 gene expression in human T-cell leukemia virus-I-infected patients offers new prospects for therapy. *Blood.* 1998;91(7):2467-2474.
7. Ohno N, Tani A, Uozumi K, et al. Expression of functional lung resistance: related protein predicts poor outcome in adult T-cell leukemia. *Blood.* 2001;98(4):1160-1165.
8. Okamura J, Utsunomiya A, Tanosaki R, et al. Allogeneic stem-cell transplantation with reduced conditioning intensity as a novel immunotherapy and antiviral therapy for adult T-cell leukemia/lymphoma. *Blood.* 2005;105(10):4143-4145.
9. Fukushima T, Miyazaki Y, Honda S, et al. Allogeneic hematopoietic stem cell transplantation provides sustained long-term survival for patients with adult T-cell leukemia/lymphoma. *Leukemia.* 2005;19(5):829-834.
10. Matutes E, Taylor GP, Cavenagh J, et al. Interferon alpha and zidovudine therapy in adult T-cell leukaemia lymphoma: response and outcome in 15 patients. *Br J Haematol.* 2001;113(3):779-784.
11. Hermine O, Allard I, Lévy V, Arnulf B, et al. A prospective phase II clinical trial with the use of zidovudine and interferon-alpha in the acute and lymphoma forms of adult T-cell leukemia/lymphoma. *Hematol J.* 2002;3(6):276-282.
12. Ohashi T, Hanabuchi S, Kato H, et al. Prevention of adult T-cell leukemia-like lymphoproliferative disease in rats by adoptively transferred T cells from a donor immunized with human T-cell leukemia virus type 1 Tax-coding DNA vaccine. *J Virol.* 2000;74(20):9610-9616.
13. Akimoto M, Kozako T, Sawada T, et al. Anti-HTLV-1 tax antibody and tax-specific cytotoxic T lymphocyte are associated with a reduction in HTLV-1 proviral load in asymptomatic carriers. *J Med Virol.* 2007;79(7):977-986.
14. Mori N, Yamada Y, Ikeda S, et al. Bay 11-7082 inhibits transcription factor NF-kappaB and induces apoptosis of HTLV-I-infected T-cell lines and primary adult T-cell leukemia cells. *Blood.* 2002;100(5):1828-1834.
15. Dewan MZ, Uchihara JN, Terashima K, et al. Efficient intervention of growth and infiltration of primary adult T-cell leukemia cells by an HIV protease inhibitor, ritonavir. *Blood.* 2006;107(2):716-724.
16. Mitra-Kaushik S, Harding JC, Hess JL, et al. Effects of the proteasome inhibitor PS-341 on tumor growth in HTLV-1 Tax transgenic mice and Tax tumor transplants. *Blood.* 2004;104(3):802-809.
17. Liu Y, Wang Y, Yamakuchi M, et al. Phosphoinositide-3 kinase-PKB/Akt pathway activation is involved in fibroblast Rat-1 transformation by human T-cell leukemia virus type I tax. *Oncogene.* 2001;20(20):2514-2526.
18. Ikezoe T, Nishioka C, Bandobashi K, et al. Longitudinal inhibition of PI3K/Akt/mTOR signaling by LY294002 and rapamycin induces growth arrest of adult T-cell leukemia cells. *Leuk Res.* 2007; 31(5):673-682.
19. Brown M, Bellon M, Nicot C. Emodin and DHA potently increase arsenic trioxide interferon-alpha-induced cell death of HTLV-I-transformed cells by generation of reactive oxygen species and inhibition of Akt and AP-1. *Blood.* 2007; 109(4):1653-1659.
20. Taylor JM, Nicot C. HTLV-1 and apoptosis: role in cellular transformation and recent advances in therapeutic approaches. *Apoptosis.* 2008;13(6): 733-747.
21. Waldmann TA. Anti-Tac (daclizumab, Zenapax) in the treatment of leukemia, autoimmune diseases, and in the prevention of allograft rejection: a 25-year personal odyssey. *J Clin Immunol.* 2007; 27(1):1-18.
22. Zhang Z, Zhang M, Goldman CK, et al. Effective therapy for a murine model of adult T-cell leukemia with the humanized anti-CD52 monoclonal antibody, Campath-1H. *Cancer Res.* 2003; 63(19):6453-6457.
23. Ishida T, Iida S, Akatsuka Y, et al. The CC chemokine receptor 4 as a novel specific molecular target for immunotherapy in adult T-cell leukemia/lymphoma. *Clin Cancer Res.* 2004;10(22):7529-7539.
24. Lieberman HB. DNA damage repair and response proteins as targets for cancer therapy. *Curr Med Chem.* 2008;15(4):360-367.
25. Martin SA, Lord CJ, Ashworth A. DNA repair deficiency as a therapeutic target in cancer. *Curr Opin Genet Dev.* 2008;18(1):80-86.
26. Helleday T, Petermann E, Lundin C, et al. DNA repair pathways as targets for cancer therapy. *Nat Rev Cancer.* 2008;8(3):193-204.
27. Hakem R. DNA-damage repair; the good, the bad, and the ugly. *EMBO J.* 2008;27(4):589-605.
28. Burma S, Chen DJ. Role of DNA-PK in the cellular response to DNA double-strand breaks. *DNA Repair (Amst).* 2004;3(8-9):909-918.
29. Abe T, Ishiai M, Hosono Y, et al. KU70/80, DNA-PKcs, and Artemis are essential for the rapid induction of apoptosis after massive DSB formation. *Cell Signal.* 2008;20(11):1978-1985.
30. Guo L, Liu X, Nishikawa K, et al. Inhibition of topoisomerase IIalpha and G_2 cell cycle arrest by NK314, a novel benzo[c]phenanthridine currently in clinical trials. *Mol Cancer Ther.* 2007;6(5): 1501-1508.
31. Onda T, Toyoda E, Miyazaki O, et al. NK314, a novel topoisomerase II inhibitor, induces rapid DNA double-strand breaks and exhibits superior antitumor effects against tumors resistant to other topoisomerase II inhibitors. *Cancer Lett.* 2008; 259(1):99-110.
32. Toyoda E, Kagaya S, Cowell IG, et al. NK314, a topoisomerase II inhibitor that specifically targets the alpha isoform. *J Biol Chem.* 2008;283(35): 23711-23720.
33. Naoe T, Akao Y, Yamada K, et al. Cytogenetic characterization of a T-cell line, ATN-1, derived from adult T-cell leukemia cells. *Cancer Genet Cytogenet.* 1988;34(1):77-88.
34. Yamada Y, Fujita M, Suzuki H, et al. Established IL-2-dependent double-negative (CD4- CD8-) TCR alpha beta/CD3+ ATL cells: induction of CD4 expression. *Br J Haematol.* 1994;88(2):234-241.
35. Yamada Y, Ohmoto Y, Hata T, et al. Features of the cytokines secreted by adult T cell leukemia (ATL) cells. *Leuk Lymphoma.* 1996;21(5):443-447.
36. Miyoshi I, Kubonishi I, Sumida M, et al. A novel T-cell line derived from adult T-cell leukemia. *Gann.* 1980;71(1):155-156.
37. Miyoshi I, Kubonishi I, Yoshimoto S, et al. Type C virus particles in a cord T-cell line derived by cocultivating normal human cord leukocytes and human leukaemic T cells. *Nature.* 1981; 294(5843):770-771.
38. Yamada Y, Sugawara K, Hata T, et al. Interleukin-15 (IL-15) can replace the IL-2 signal in IL-2-dependent adult T-cell leukemia (ATL) cell lines: expression of IL-15 receptor alpha on ATL cells. *Blood.* 1998;91(11):4265-4272.
39. Kurimasa A, Kumano S, Boubnov NV, et al. Requirement for the kinase activity of human DNA-dependent protein kinase catalytic subunit in DNA strand break rejoining. *Mol Cell Biol.* 1999; 19(5):3877-3884.
40. Iwanaga K, Sueoka N, Sato A, et al. Heterogeneous nuclear ribonucleoprotein B1 protein impairs DNA repair mediated through the inhibition of DNA-dependent protein kinase activity. *Biochem Biophys Res Commun.* 2005;333(3): 888-895.
41. Clarke DJ, Vas AC, Andrews CA, et al. Topoisomerase II checkpoints: universal mechanisms that regulate mitosis. *Cell Cycle.* 2006;5(17):1925-1928.
42. Veuger SJ, Curtin NJ, Smith GC, et al. Effects of novel inhibitors of poly(ADP-ribose) polymerase-1 and the DNA-dependent protein kinase on enzyme activities and DNA repair. *Oncogene.* 2004;23(44):7322-7329.
43. Ryu JS, Um JH, Kang CD, et al. Fractionated irradiation leads to restoration of drug sensitivity in MDR cells that correlates with down-regulation of P-gp and DNA-dependent protein kinase activity. *Radiat Res.* 2004;162(5):527-535.
44. Deriano L, Guipaud O, Merle-Béral H, et al. Human chronic lymphocytic leukemia B cells can escape DNA damage-induced apoptosis through the nonhomologous end-joining DNA repair pathway. *Blood.* 2005;105(12):4776-4783.
45. Zhao Y, Thomas HD, Batey MA, et al. Preclinical evaluation of a potent novel DNA-dependent protein kinase inhibitor NU7441. *Cancer Res.* 2006; 66(10):5354-5362.
46. Willmore E, Elliott SL, Mainou-Fowler T, et al. DNA-dependent protein kinase is a therapeutic target and an indicator of poor prognosis in B-cell chronic lymphocytic leukemia. *Clin Cancer Res.* 2008;14(12):3984-3992.
47. Shao CJ, Fu J, Shi HL, et al. Activities of DNA-PK and Ku86, but not Ku70, may predict sensitivity to cisplatin in human gliomas. *J Neurooncol.* 2008; 89(1):27-35.
48. Marriott SJ, Semmes OJ. Impact of HTLV-I Tax on cell cycle progression and the cellular DNA damage repair response. *Oncogene.* 2005;24(39): 5986-5995.
49. Durkin SS, Guo X, Fryrear KA, et al. HTLV-1 Tax oncoprotein subverts the cellular DNA damage response via binding to DNA-dependent protein kinase. *J Biol Chem.* 2008;283(52):36311-36320.
50. Noronha V, Berliner N, Ballen KK, et al. Treatment-related myelodysplasia/AML in a patient with a history of breast cancer and an oligodendroglioma treated with temozolomide: case study and review of the literature. *Neuro Oncol.* 2006; 8(3):280-283.
51. Hijiya N, Ness KK, Ribeiro RC, et al. Acute leukemia as a secondary malignancy in children and adolescents: current findings and issues. *Cancer.* 2009;115(1):23-35.
52. Deweese JE, Osheroff N. The DNA cleavage reaction of topoisomerase II: wolf in sheep's clothing. *Nucleic Acids Res.* 2009;37(3):738-748.
53. Zeiser R, Negrin RS. Interleukin-2 receptor downstream events in regulatory T cells: implications for the choice of immunosuppressive drug therapy. *Cell Cycle.* 2008;7(4):458-462.

Human Molecular Genetics, 2011, Vol. 20, No. 19 **3798–3810**
doi:10.1093/hmg/ddr298
Advance Access published on July 1, 2011

Neuron-specific impairment of inter-chromosomal pairing and transcription in a novel model of human 15q-duplication syndrome

Makiko Meguro-Horike[1], Dag H. Yasui[2], Weston Powell[2], Diane I. Schroeder[2], Mitsuo Oshimura[3], Janine M. LaSalle[2] and Shin-ichi Horike[1,*]

[1]Frontier Science Organization, Kanazawa University, 13-1 Takaramachi, Kanazawa 920-0934, Japan, [2]Department of Medical Microbiology and Immunology, Genome Center and M.I.N.D. Institute, University of California Davis School of Medicine, 1 Shields Avenue Davis, CA 95616, USA and [3]Department of Biomedical Science, Tottori University, 86 Nishi-cho, Yonago, Tottori 683-8503, Japan

Received April 3, 2011; Revised June 25, 2011; Accepted June 28, 2011

Although the etiology of autism remains largely unknown, cytogenetic and genetic studies have implicated maternal copy number gains of 15q11–q13 in 1–3% of autism cases. In order to understand how maternal 15q duplication leads to dysregulation of gene expression and altered chromatin interactions, we used microcell-mediated chromosome transfer to generate a novel maternal 15q duplication model in a human neuronal cell line. Our 15q duplication neuronal model revealed that by quantitative RT–PCR, transcript levels of *NDN*, *SNRPN*, *GABRB3* and *CHRNA7* were reduced compared with expected levels despite having no detectable alteration in promoter DNA methylation. Since 15q11–q13 alleles have been previously shown to exhibit homologous pairing in mature human neurons, we assessed homologous pairing of 15q11–q13 by fluorescence *in situ* hybridization. Homologous pairing of 15q11–q13 was significantly disrupted by 15q duplication. To further understand the extent and mechanism of 15q11–q13 homologous pairing, we mapped the minimal region of homologous pairing to a ~500 kb region at the 3′ end of *GABRB3* which contains multiple binding sites for chromatin regulators MeCP2 and CTCF. Both active transcription and the chromatin factors MeCP2 and CTCF are required for the homologous pairing of 15q11–q13 during neuronal maturational differentiation. These data support a model where 15q11–q13 genes are regulated epigenetically at the level of both inter- and intra-chromosomal associations and that chromosome imbalance disrupts the epigenetic regulation of genes in 15q11–q13.

INTRODUCTION

Autism spectrum disorders (ASDs; MIM 209850) include a complex group of neurodevelopmental disorders characterized by impairments in reciprocal social interactions, problems in communication and a restricted range of behaviors and interests. ASD affects individuals of all socio-economic and cultural backgrounds and has a prevalence of 6 per 1000 individuals, with males affected four times more frequently than females (1,2). There is compelling evidence for a genetic etiology of ASD from twin studies that have shown high concordance between monozygotic twins (3–5). To date, cytogenetic studies have identified a number of pathogenic chromosomal anomalies in ASD patients (1). In addition, current microarray-based technologies have enabled the detection of submicroscopic microdeletions and microduplications [copy number variations (CNVs)] and revealed that submicroscopic CNVs can have a pathogenic role in ASD as well (3,4). Human chromosome 15q11–q13 is frequently involved in clinically important genomic rearrangements, including interstitial deletions, duplications and supernumerary marker chromosome, called isodicentric chromosome (idic) (5). After fragile X, maternal 15q11–q13 duplications are the most common cytogenetic cause of autism, occurring in ~1–3% of individuals with ASD (6–9). A recent analysis of 10K single-nucleotide polymorphism data identified 15q11–q13 CNVs in 17 of 1749 autism patients (10).

*To whom correspondence should be addressed. Tel: +81 762652775; Fax: +81 762344537; Email: sihorike@staff.kanazawa-u.ac.jp

Genomic imprinting is an epigenetic mechanism that establishes parent-of-origin-specific gene expression patterns. Deletions of 15q11–q13 on the paternal chromosome 15 cause Prader–Willi syndrome (PWS; MIM 176270), whereas maternal deletions cause Angelman syndrome (AS; MIM 105830) (11). Parental differences in DNA methylation at imprinting control regions have a crucial role in genomic imprinting of 15q11–q13, as well as differences in DNA replication timing, histone modifications, chromosome nuclear organization and mitotic recombination frequencies (12). However, despite progress in molecular characterization of 15q11–q13 rearrangements and imprinting mechanisms, the molecular pathogenesis of the autism phenotype resulting from maternal 15q11–q13 duplications remains largely unknown. The ubiquitin E3 ligase gene *UBE3A* is the primary candidate gene presumed to be dysregulated in 15q duplication syndrome because of imprinted maternal expression in the brain. In particular, *UBE3A* has been analyzed due to its role in AS, its pattern of imprinting and its biological function (13–15). However, 15q11–q13 duplications also include the cluster of three gamma-aminobutyric acid A receptor ($GABA_AR$) subunit genes (*GABRB3, GABRA5, GABRG3*) and paternally expressed genes implicated in splicing (*SNRPN*), circadian rhythm (*MAGEL2*), respiration (*NDN*) and nucleolar function (*HBII85, HBII52*) (16,17). While increased copy number of 15q11–q13 was predicted to increase expression of the maternally expressed *UBE3A* and biallelically expressed genes such as *GABRB3* and *GABRA5*, prior investigation of an idic15 brain sample with PWS-like features instead showed reduced levels of *GABRB3*, *GABRA5*, *GABRG3*, *SNRPN*, *HBII85* and *HBII52* (18). The striking parent-of-origin pattern of inheritance for 15q11–q13 rearrangements has led to the hypothesis that higher order epigenetic dysregulation of transcription within this region may be involved in ASD.

The higher order, inter-chromosomal association of homologous pairing of maternal and paternal alleles of 15q11–q13 was originally described in lymphocytes and predicted to regulate maintenance of imprinting in the locus (19). Homologous pairing of 15q11–q13 was shown to occur in neurons and be deficient in brains of individuals with Rett syndrome (RTT; MIM 312750), autism and maternal 15q duplication (18,20). Although these observations raise the possibility that homologous pairing of 15q11–q13 is an important spatial organization modulating neuron-specific transcripts within the paired regions, the mechanisms of homologous pairing and its effects on gene expression within the paired regions in neurons has not been previously determined.

Here, we made use of microcell-mediated chromosome transfer (MMCT) technology to generate a 15q11–q13 maternal duplication model in a human neuronal cell line. Using this MMCT method, a maternal copy of human chromosome 15 was successfully transferred into human SH-SY5Y neuronal cells. Our experimental models of 15q duplication syndrome recapitulated the reduced levels of several transcripts resulting from increased maternal 15q11–q13 dosage previously observed in the brain as well as the reduced homologous pairing. We further show that the chromatin regulators MeCP2 and CTCF are required for the homologous pairing of 15q11–q13 during neuronal differentiation. These results provide insight into the inter- and intra-chromosomal spatial interactions influencing 15q11–q13 transcript levels in neurons and provide support for an epigenetic dysregulation pathway by which 15q11–q13 duplications may result in ASD.

RESULTS

Establishment of a maternal 15q duplication model by microcell fusion

We have previously established mouse A9 hybrid cells retaining a single human chromosome of defined parental origin for the investigation of imprinted loci in humans (21). Gene expression and DNA methylation studies demonstrated that the appropriate imprinting status of human loci was maintained in mouse A9 hybrids (22–24). In this study, to generate a novel maternal 15q duplication model in a neuronal cell line, a maternal human chromosome 15 was transferred from mouse A9 hybrids into human SH-SY5Y neuronal cells by MMCT (Fig. 1A). SH-SY5Y cells were selected as a recipient cell line because they can be induced to undergo differentiation within 72 h using PMA, resulting in a morphologic change in the extension of axonal projections and the increased expression of neuron-specific enolase (25). In addition, SH-SY5Y cells are diploid for most chromosomes (26). Our PCR-restriction fragment length polymorphism (RFLP) analysis identified 20 independent SH-SY5Y microcell hybrids that contained an extra maternal copy of human chromosome 15, and therefore named SH(15M) cell lines (Fig. 1B). To further confirm the state of the introduced maternal human chromosome 15 in SH-SY5Y cells, we performed cytogenetic analyses using fluorescence *in situ* hybridization (FISH) (Fig. 1C). Finally, we confirmed that introduced maternal chromosome 15 was maintained stably in SH(15M) cell lines under appropriate selection conditions. For further analyses, we selected three independent SH(15M) cell lines that morphologically resembled parental SH-SY5Y cells.

Quantitation of 15q11–q13 transcripts in a maternal 15q duplication model

To determine the effect of increased maternal chromosome 15 dosage on transcript levels in SH(15M) cells, quantitative RT–PCR was used to measure the levels of eight transcripts at the 15q11–q13 locus and two non-15q11–q13 housekeeping gene controls, *GAPDH* and *ACTB* (Fig. 2A). The non-imprinted genes *CYFIP1* and *TJP1* revealed the expected 1.5-fold increase in transcript abundance in all three SH(15M) cell lines (Fig. 2B and C). In contrast, expression of non-imprinted *GABRB3* and *CHRNA7* genes was significantly reduced compared with the parental cell line in all three SH(15M) lines, despite increased 15q11–q13 dosage (Fig. 2D and E). Moreover, paternal expression of *NDN* and *SNRPN* transcripts was also significantly reduced despite the increased maternal dosage (Fig. 2F and G). Furthermore, there was no difference between control SH-SY5Y cells and SH(15M) cells in the levels of maternally expressed *UBE3A* transcript, even though a 2-fold increase was expected

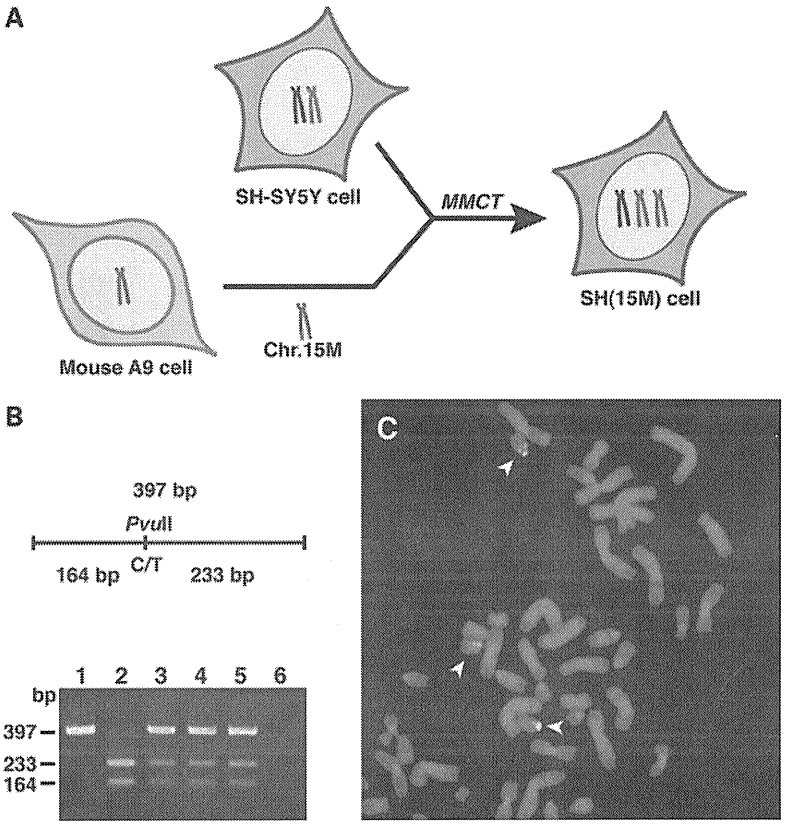

Figure 1. Characterization of SH-SY5Y neuronal cells containing an extra maternal human chromosome 15. (**A**) A schematic diagram showing the construction of SH-SY5Y microcell hybrids [SH(15M) cell] containing an extra maternal copy of human chromosome 15. Transfer of a maternal human chromosome 15 from mouse A9 cells to SH-SY5Y cell was performed by MMCT technology. (**B**) RFLP analysis to confirm presence of donor chromosome 15 in SH(15M) cells is shown. DNA from introduced maternal human chromosome 15 donor A9 cells (lane 1), SH-SY5Y cells (lane 2), SH(15M)-1, 2, 3 cells (lanes 3–5) and mouse A9 cells (lane 6) was amplified by PCR using primers that span a *Pvu*II polymorphism. Both chromosome 15 copies in the host SH-SY5Y cells were digested by *Pvu*II, but the donor chromosome 15 was undigested. SH(15M) cells contained both digested and undigested fragments. (**C**) Results from DNA-FISH analysis of SH(15M) cells. Metaphase chromosomes from SH(15M) were hybridized *in situ* with Vysis LSI *GABRB3* (red) and CEP15 (green) probes. The arrowheads indicate three copies of chromosome 15.

(Fig. 2H). In addition, another maternally expressed gene, *ATP10A*, was also significantly reduced despite the increased maternal dosage (Fig. 2I). While extra copies of genes are expected to result in increased transcript levels, our SH(15M) cell lines recapitulated the direction of transcriptional alterations previously observed in a human brain sample with maternal 15q duplication (18).

We next assessed the DNA methylation status of *NDN, SNRPN, UBE3A, GABRB3* and *CHRNA7* promoter CpG islands by bisulfite sequencing to determine whether the DNA methylation status of these promoters was correlated with the observed reductions in transcript levels. *GABRB3, CHRNA7* and *UBE3A* promoters in the SH(15M) cells were almost completely unmethylated and appeared similar to those observed in control SH-SY5Y cells (Supplementary Material, Fig. S1A–C). Similarly, the expected maternal DNA methylation levels were observed for *NDN* and *SNRPN* promoter CpG islands in both SH-SY5Y cells and SH(15M) cells (Supplementary Material, Fig. S1D and E). Because these CpG islands are differentially methylated in a parent-of-origin-specific manner, increased DNA methylation levels were expected following chromosome transfer of the methylated maternal allele (27,28). A combined bisulfite restriction analysis (29) showed strong concordance with bisulfite sequencing results (data not shown). These findings indicate that promoter DNA methylation is not correlated with altered transcript levels of *NDN, SNRPN, UBE3A, GABRB3* or *CHRNA7* in SH(15M) cells.

Disruption of 15q11–q13 homologous pairing in a maternal 15q duplication model

Homologous chromosomal association or pairing of maternal and paternal 15q11–q13 alleles has previously been described in both lymphocytes (19) and neurons (20) and disrupted in the 15q dup brain (18). Therefore, we investigated the impact of an extra maternal human chromosome 15 on normal interactions between maternal and paternal 15q11–q13 alleles. In comparison with SH-SY5Y cells, SH(15M) cells displayed a significant reduction in the percentage of paired alleles for nuclei hybridized with a Vysis LSI *GABRB3* probe (Fig. 3A and B). However, there was no difference in the percentage of paired alleles of nuclei hybridized with a control chromosome 15 pericentromeric CEP15 probe. Homologous pairing was

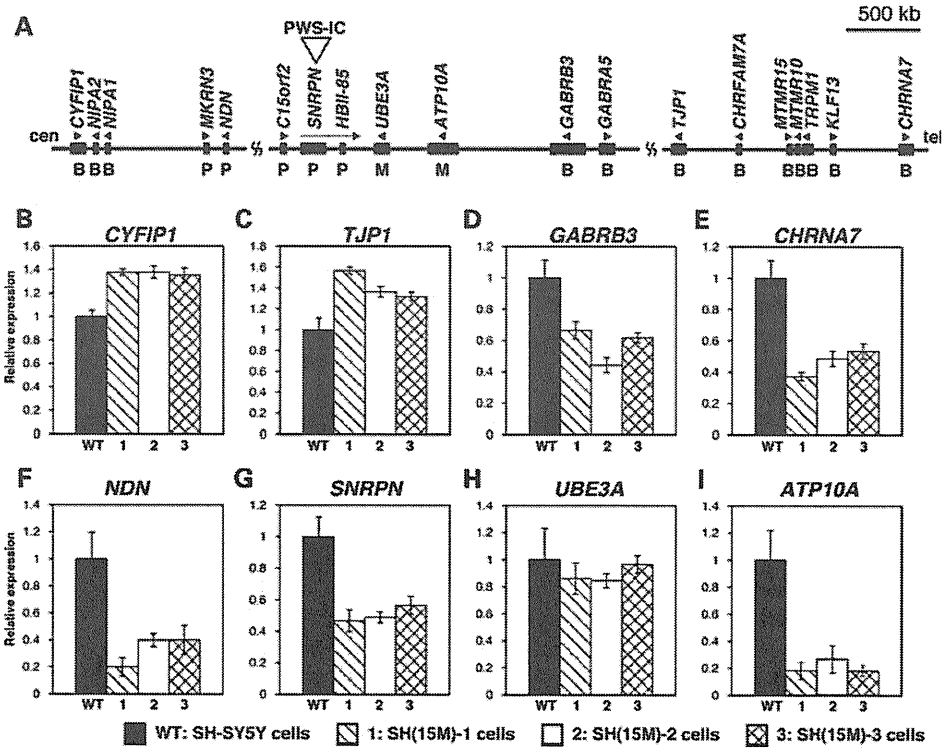

Figure 2. Analysis of 15q11–q13 transcript levels in experimental model of dup15q syndrome. (**A**) Physical map of the imprinted gene cluster in human chromosome 15q11–q13. PWS-IC is the PWS imprinting center, which is essential for establishment of the paternal epigenetic state of the region. Genes or transcripts (filled boxes) are drawn approximately to scale. Transcriptional direction is indicated by arrowheads and arrows. P, paternally expressed genes; M, maternally expressed genes; B, biallelically expressed genes. (**B–I**) Summary of quantitative RT–PCR measurements of eight transcripts in 15q11–q13, normalized to the housekeeping genes *GAPDH* and *ACTB*. Error bars represent ± SEM. All qRT–PCR analyses were performed on cDNA from PMA-treated differentiated SH-SY5Y cells (WT) and PMA-treated differentiated SH(15M) cells (1–3). (B)–(E) are non-imprinted biallelically expressed genes, (F) and (G) are paternally expressed imprinted genes and (H) and (I) are maternally expressed imprinted genes.

not observed in either SH-SY5Y or SH(15M) cells hybridized with a non-15 control, a pericentromeric probe specific for chromosome 11 (CEP11; data not shown). Thus, the extra maternal human chromosome 15 in the SH(15M) cells conferred a specific effect on the nuclear organization of 15q11–q13 and modeled the homologous pairing defect previously observed in the 15q duplication syndrome brain (18). In addition, our observations indicate that homologous pairing of 15q11–q13 could influence gene expression within the paired region.

Homologous pairing of 15q11–q13 in the 3′ region of the *GABRB3* gene

The mechanism of homologous pairing of 15q11–q13 in neurons is poorly understood, but critical for understanding the changes in transcription that accompany the loss of homologous pairing in 15q duplication syndrome. To map the precise location and extent of 15q11–q13 homologous pairing upon neuronal differentiation, we performed additional FISH analyses using nine different fluorescently labeled bacterial artificial chromosome (BAC) probes distributed over 9 Mb of 15q11–q13 (Fig. 4A). We measured the inter-chromosomal distances between FISH signals from each BAC probe both before (untreated) and 72 h after differentiation with PMA (PMA treated) (20). In comparison with undifferentiated SH-SY5Y cells, a high percentage of nuclei displayed close inter-chromosomal distances (2 μm or less) at the *GABRB3* locus following neuronal differentiation, as shown by a significant leftward shift in the distribution (Fig. 4B–E). In contrast to the significant decrease observed in inter-chromosome distances at *GABRB3*, the *CYFIP* locus showed the opposite pattern, with a significant increase in inter-chromosome distance following differentiation (Fig. 4B–D).

To narrow down the genomic region in which the homologous inter-chromosomal association was observed, we performed detailed frequency analyses of homologous allele distances across the $GABA_AR$ subunit gene cluster (Fig. 5A). Homologous pairing of 15q11–q13 was observed in the 3′ region of the *GABRB3* gene, but not in *GABRA5* and *GABRG3* (Fig. 5B–D). This in-depth analysis of multiple FISH probes therefore narrowed the locus of homologous interaction to a ~500 kb region at the 3′ end of *GABRB3*, with significant changes in homologous pairing during SH-SY5Y differentiation limited to the region detected by a single BAC probe, GABRB3(2).

Because clustering of *$GABA_AR$* subunit genes is well conserved on human chromosomes 4, 5, 15 and X, it has previously been hypothesized that the physical proximity of $GABA_AR$ subunit genes facilitates temporally and spatially coordinated expression (30). Therefore, we wished to test whether the homologous chromosomal association is also conserved in other clusters of *$GABA_AR$* subunit genes. To this end, the homologous

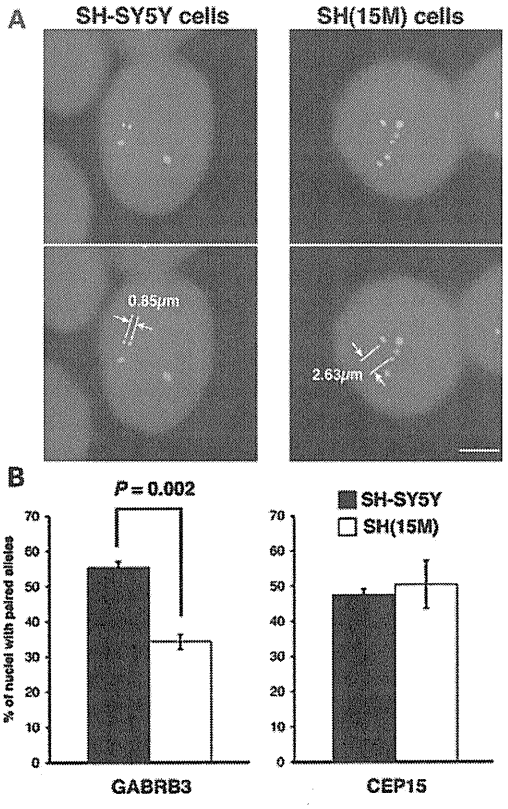

Figure 3. Reduced homologous pairing of *GABRB3* alleles as a result of duplicated maternal chromosome 15 in SH-SY5Y cells. (**A**) Representative image of chr.15–chr.15 localization in SH-SY5Y cells (left panel) and SH(15M) cells (right panel) using Vysis LSI *GABRB3* SpectrumOrange/CEP15 SpectrumGreen. The iVision software was used to measure distances between two signals. In case of SH(15M) cells, we measured the shortest interchromosomal distances between the three signals. Scale bars: 5 μm. (**B**) Differences in homologous pairing in SH-SY5Y cells (gray bars) and SH(15M) cells (white bars), as determined by hybridization with Vysis LSI *GABRB3* (left panel) and CEP15 (right panel) FISH probes. Pairing was scored as homologous FISH signals with distances ≤2 μm apart. The bars indicate the mean ± SEM of three replicate experiments, in each of which 100–150 nuclei were scored. Significantly fewer SH(15M) cell nuclei showed pairing when the *GABRB3* probe was used. In contrast, no significant difference was observed in SH(15M) cells in pairing between alleles detected by the pericentromeric CEP15 probe.

pairing analyses were extended to $GABA_AR$ subunit genes on 4p12 and 5q34 (Supplementary Material, Fig. S2). Unlike 15q11–q13, homologous pairings of 4p12 and 5q34 were not observed during neuronal differentiation. However, transcript levels for *GABRG1* and *GABRA4* on 4p12, and *GABRG2* and *GABRA6* on 5q34 were barely detectable in differentiated SH-SY5Y cells (data not shown). Cumulatively, our findings suggest that homologous chromosomal pairing in 15q11–q13 coincides with increased expression of $GABA_AR$ subunit genes specifically in this locus during neuronal differentiation, as *GABRB3* is highly expressed in differentiated SH-SY5Y cells (data not shown). Therefore, in order to investigate whether active transcription is necessary for homologous chromosomal pairing in 15q11–q13, differentiated SH-SY5Y cells were treated with the transcriptional inhibitor α-amanitin. The observation that α-amanitin caused significant decreases in the percentage of paired alleles for nuclei hybridized with *GABRB3* probe suggests that active transcription was required for homologous chromosomal pairing in 15q11–q13 (Fig. 4F).

Involvement of chromatin proteins MeCP2 and CTCF in regulation of 15q11–q13 homologous pairing

Our observations raise the question as to which factors control the homologous pairing of 15q11–q13. Notably, we observed multiple binding sites for MeCP2 and CTCF in a ~500 kb region between at the 3′ end of *GABRB3*. We used a short-interfering RNA (siRNA)-mediated knockdown approach to directly test the role of MeCP2 in the homologous pairing of 15q11–q13 by transiently depleting MeCP2 expression. MeCP2 protein depletion in differentiated SH-SY5Y cells was confirmed by western blot analysis and immunostaining (Fig. 6A–C) and chr.15–chr.15 interchromosomal distances were measured between FISH signals of GABRB3 and CEP15 probes (Fig. 6D). Consistent with previous findings, homologous pairing at *GABRB3* was significantly reduced in MeCP2 knockdown cells compared with non-targeting siRNA-treated cells (20). Specifically, the two GABRB3 FISH signals were ≤2 μm apart in only 18.5% of MeCP2-deficient nuclei compared with 48.9% in control cells.

CTCF is also required for inter- and intra-chromosomal associations during genomic imprinting and X inactivation (31–34). A chromatin immunoprecipitation assay using a CTCF-specific antibody demonstrated that there are three CTCF-binding sites at the 3′ region of the *GABRB3* gene (Supplementary Material, Fig. S3). Therefore, we examined whether CTCF deficiency affected homologous pairing at the *GABRB3* locus in differentiated SH-SY5Y cells. Western blot and immunostaining analyses showed that CTCF was predominantly depleted at the protein level (Fig. 6E–G). Interestingly, depletion of CTCF resulted in a significant reduction in the homologous pairing at *GABRB3*, and at CEP15 (Fig. 6H). In contrast, knocking down RAD21 had no obvious effect on the homologous pairing of 15q11–q13 (Supplementary Material, Fig. S4), although this protein has been reported to frequently accumulate at CTCF-binding sites (35). These results suggest that MeCP2 and CTCF are essential mediators for the homologous pairing of 15q11–q13.

DISCUSSION

Autism has been linked to the region on chromosome 15q11–q13 that is responsible for the imprinting disorders PWS and AS (1,3,5). Maternal 15q11–q13 duplications are the most frequent cytogenetically detectable mutation associated with ASD (6–9), but the molecular impact of 15q duplication in neurons has been difficult to assess because of the lack of an appropriate model system. While overexpression of maternally expressed *UBE3A* was predicted to be the major cause of the ASD phenotype in 15q duplication syndrome (36), Hogart and LaSalle (18) revealed that 15q11–q13 transcripts in maternal 15q11–q13 duplication brain samples were altered in a direction not predicted from maternal copy number gains. This led to the suggestion that an imbalance of 15q11–q13 dosage can disrupt normal epigenetic pathways such as parental homologous pairing and DNA methylation status, changing gene

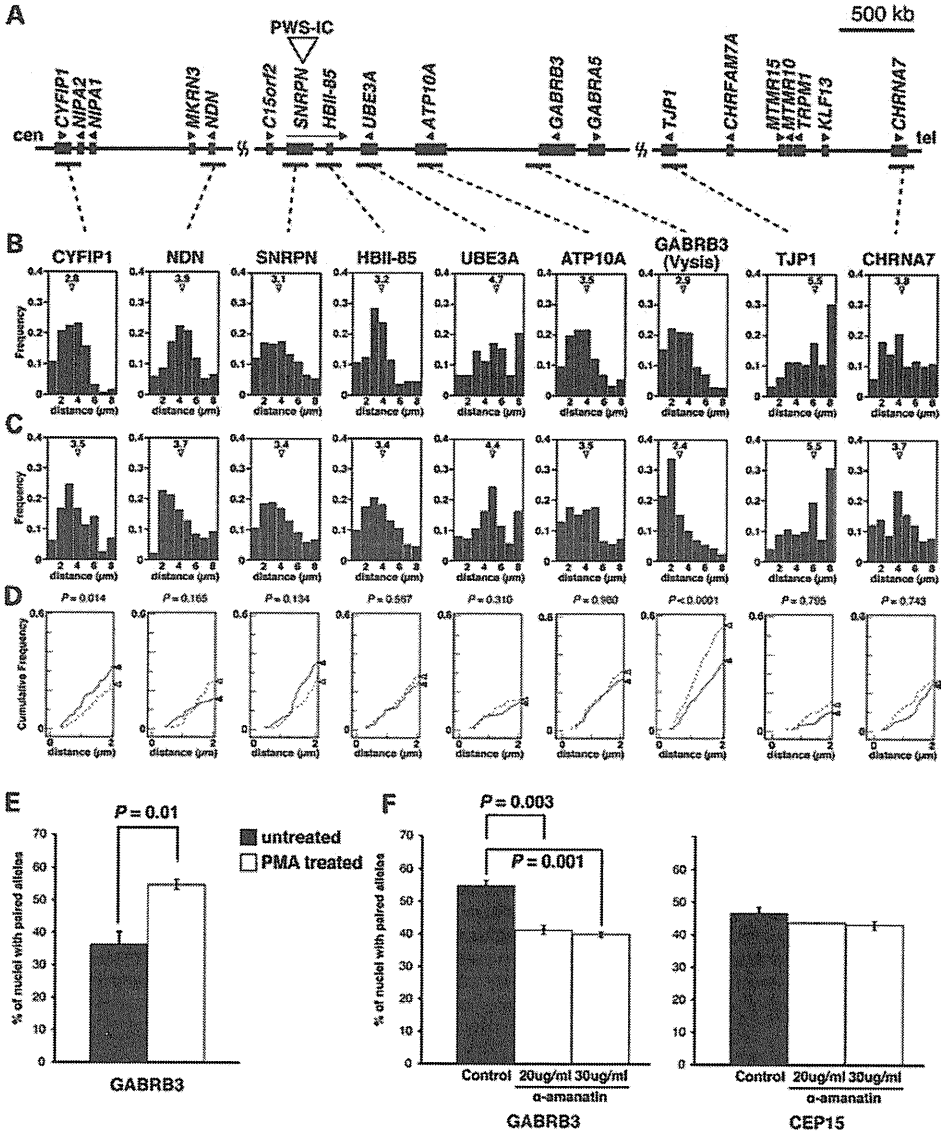

Figure 4. Increased homologous pairing of *GABRB3* alleles during neuronal differentiation is associated with active transcription. (**A**) Physical map of the imprinted gene cluster in human chromosome 15q11–q13. PWS-IC is the PWS imprinting center, which is essential for establishment of the paternal epigenetic state of the region. Genes or transcripts (filled boxes) are drawn approximately to scale. Transcriptional direction is indicated by arrowheads and arrows. The horizontal bars indicate BAC probes used in the pairing analyses. *GABRB3*(1) probe indicates the Vysis LSI *GABRB3* Spectrum Orange probe. (**B**) Frequency distribution of distances between homologous alleles at multiple sites along 15q11–q13 for undifferentiated SH-SY5Y cell nuclei, as measured on each BAC probe. Mean distance, open triangle. (**C**) Frequency distribution of distances between homologous alleles at multiple sites along 15q11–q13 for PMA-treated differentiated SH-SY5Y cell nuclei. Mean distance, open triangle. A high proportion of PMA-treated differentiated SH-SY5Y cells displayed close homologous distances ($\leq$2 μm) at *GABRB3* upon neuronal differentiation, as shown by a leftward shift in the distribution. (**D**) Cumulative distribution of distances between homologous alleles at 0–2 μm. The solid line indicates the undifferentiated SH-SY5Y cells. The dotted line indicates the PMA-treated differentiated SH-SY5Y cells. The closed and open triangles indicate cumulative frequency at 2 μm, respectively. The statistical relevance was assessed by a comparison of the entire histogram of measurement distributions from (B) and (C) using two non-parametric tests, namely Mann–Whitney's *U*-test and Kolmogorov–Smirnov test. *P*-values from Mann–Whitney's *U*-test are as indicated. Sample sizes for each experiment ranged from 100 to 210. (**E**) Differences in homologous pairing in the undifferentiated SH-SY5Y cells (gray bars) and the PMA-treated differentiated SH-SY5Y cells (white bars), as determined by hybridization with Vysis LSI G*ABRB3* FISH probes. Pairing was scored as homologous FISH signals with distances $\leq$2 μm apart. The bars indicate the mean ± SEM of three replicate experiments, in each of which 100–150 nuclei were scored. (**F**) The PMA-treated differentiated SH-SY5Y cells treated for 4 h with the transcriptional inhibitor, α-amanitin, were hybridized with Vysis LSI G*ABRB3* (left panel) and CEP15 (right panel) FISH probes and signals measured. Transcriptional inhibition resulted in a significant reduction in the homologous pairing at *GABRB3*, but not at CEP15. Student's *t*-test.

expression patterns within 15q11–q13. Indeed, our prior study showed that various autosomal imbalances commonly affect neuronal differentiation through the dysregulation of gene expression (37).

In this study, we made use of MMCT to generate a 15q11–q13 maternal duplication model in a neuronal cell line to explore the molecular basis of epigenetic dysregulation in 15q dup syndrome. Using this MMCT method, a maternal

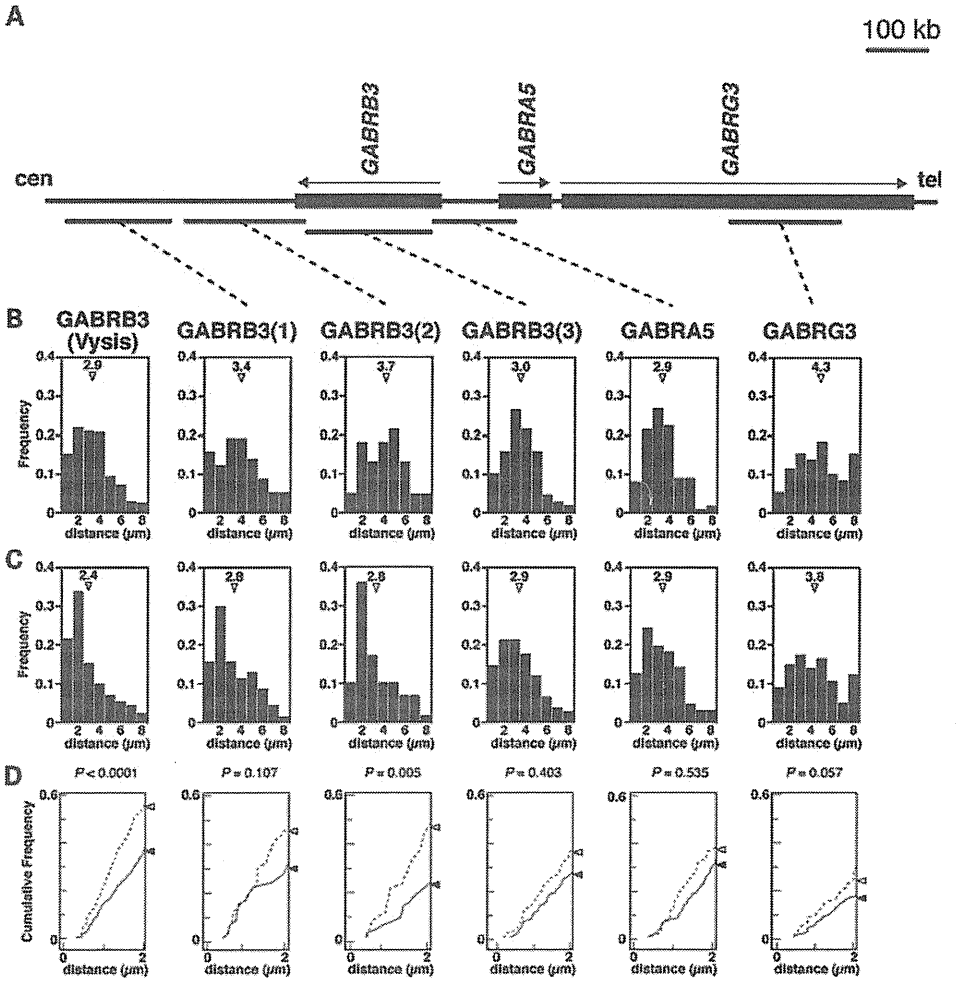

Figure 5. Homologous pairing of 15q11–q13 maps to the 3′ region of *GABRB3*. (**A**) Physical map of the cluster of *GABA$_A$R* subunit genes in 15q11–q13. The genes are drawn approximately to scale. The direction of transcription is indicated by arrows. The BAC probes used in the pairing analyses are shown by horizontal bars. (**B**) Frequency distributions of distances between homologous alleles at multiple sites along 15q11–q13 for undifferentiated SH-SY5Y cell nuclei, as measured on each BAC probe. Mean distance, open triangle. (**C**) Frequency distributions of distances between homologous alleles at multiple sites along 15q11–q13 for PMA-treated differentiated SH-SY5Y cell nuclei. A high proportion of PMA-treated differentiated SH-SY5Y cells displayed close homologous distances (≤2 μm) at *GABRB3* upon neuronal differentiation, as shown by a leftward shift in the distribution. Mean distance, open triangle. (**D**) Cumulative distance distribution for homologous alleles at 0–2 μm. The solid line indicates the undifferentiated SH-SY5Y cells. The dotted line indicates the PMA-treated differentiated SH-SY5Y cells. The closed and open triangles indicate cumulative frequency at 2 μm, respectively. The statistical relevance was assessed by a comparison of the entire histogram of measurement distributions from (B) and (C) using two non-parametric tests, namely Mann–Whitney's *U*-test and Kolmogorov–Smirnov test. *P*-values from Mann–Whitney's *U*-test are as indicated. Sample sizes for each experiment ranged from 100 to 210. One probe from the 3′ region of *GABRB3* showed significant differences in homologous intrachromosomal distance frequencies between undifferentiated SH-SY5Y cells (solid line) and the PMA-treated differentiated SH-SY5Y cells (dotted line). In contrast, one probe from the *GABRB3* gene body and two probes overlapping *GABRA5* and *GABRG3* did not show significant homologous pairing. The more centromeric GABRB3(1) probe showed a trend towards homologous pairing that was not significant.

copy of human chromosome 15 was successfully transferred into human SH-SY5Y neuronal cells. Currently, CNVs, including the 15q duplication, are beginning to provide some insights into the underlying genetic causes of neurodevelopmental disorders, in particular schizophrenia and ASD. However, the impact of CNVs on phenotypic expression remains largely unknown (38). Therefore, this study takes an important step forward by using MMCT as an important tool to define the molecular effects of CNVs in a human neuronal cell line and demonstrating that a chromosome imbalance disrupts normal homologous pairing and alters gene expression patterns.

Quantitative RT–PCR analyses revealed significant alterations in gene expression of *NDN, SNRPN, UBE3A, ATP10A, GABRB3* and *CHRNA7* in SH(15M) cells, as has previously been observed in the brains of autistic patients (18). We did not find evidence for aberrant promoter DNA methylation of these genes to explain reduced transcription. Instead, we hypothesize that higher order epigenetic alterations at the level of inter- or intra-chromosomal associations lead to transcriptional down-regulation of individual genes in the 15q11–q13 region in 15q duplication syndrome.

15q11–q13 homologous pairing appears to be a recently evolved higher order epigenetic regulatory mechanism, as it

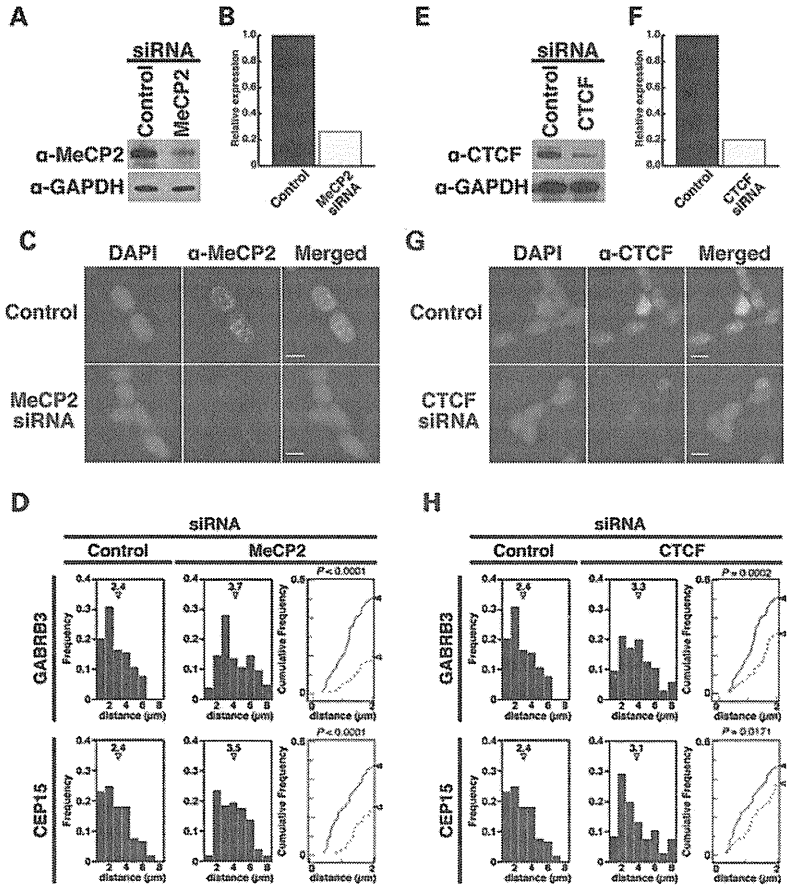

Figure 6. Disruption of *GABRB3* homologous pairing via MeCP2 and CTCF knockdown. (**A** and **E**) Results from western blot analysis confirming knockdown of MeCP2 (A) and CTCF (E) proteins in SH-SY5Y cells. (**B** and **F**) Results from western blot analysis of cell lysates after siRNA-mediated gene silencing. Both MeCP2 (B) and CTCF (F) proteins experienced ~80% knockdown. (**C** and **G**) Expression of MeCP2 (C) and CTCF (G) proteins in siRNA-treated differentiated SH-SY5Y cells. Scale bars: 10 μm. (**D** and **H**) Chr.15–Chr.15 distribution profiles and cumulative frequency curves of MeCP2 (D) and CTCF (H) in siRNA-treated differentiated SH-SY5Y cell nuclei. Mann–Whitney's *U*-test and Kolmogorov–Smirnov tests were used to determine whether the differences between the curves of the siRNA-treated cells (dotted lines) and the non-targeting siRNA-treated SH-SY5Y cells (solid lines) were significant. The statistical relevance was assessed by comparing whole histograms. *P*-values from Mann–Whitney's *U*-test are as indicated. Sample sizes for each experiment ranged from 103 to 105.

does not occur in the syntenic region in the mouse brain (20) or in lymphocytes of gorilla (39). In this study, we also found no obvious evidence for homologous pairing at the *Gabrb3* locus in mouse neurons (Supplementary Material, Fig. S5). As previously suggested elsewhere, the most likely explanation for this discrepancy is that mouse 7qC (which is homologous to the 15q11–q13 region) is not adjacent to ribosomal DNA (rDNA) genes as it is for the acrocentric human chromosome 15 (20). In addition, the *GABRB3* minimal pairing region defined in this study is highly conserved in chimp but not in mouse. These mouse–human discrepancies could begin to explain why the mouse model of 15q duplication syndrome unexpectedly showed an autism-like phenotype upon paternal transmission in opposition to what is observed in human 15q duplication patients (40). Cumulatively, these findings suggest that there has been some divergence in the genetic and/or epigenetic mechanisms relevant to homologous pairing in the human 15q11–q13 and mouse 7qC regions with potential relevance to autism.

While the proximity of *GABRB3* to the rDNA repeats on chromosome 15 may have been important in the recent evolution of homologous pairing of this locus, our study has shown that *GABRB3* pairing cannot simply be explained as a byproduct of the perinucleolar organization of acrocentric chromosomes in humans, as has been previously suggested (39). Interestingly, while both *CEP15* and *GABRB3* regions showed pairing, the effect of additional copy number of chromosome 15 on disrupting pairing was specific to *GABRB3*, not the rDNA adjacent *CEP15*, suggesting specificity to the *GABRB3* pairing beyond the acrocentric effect. Furthermore, the single gene locus most proximal to the rDNA repeats, *CYFIP*, actually exhibited increased interchromosomal distances with SH-SY5Y differentiation, suggesting that neuronal differentiation induced dynamic locus-dependent chromatin changes that were not simply rDNA proximity effects. Lastly, while transcriptional inhibition reduced *GABRB3* pairing, it had no significant effect on pairing at *CEP15*, demonstrating that *GABRB3* pairing was an active occurrence independent from rDNA organization on human 15q11–q13.

The loss of homologous pairing in the SH(15M) neuronal model led us to investigate the mechanism of homologous pairing in the 15q11–q13 region and its relation to autism

candidate genes. We narrowed down the region of homologous pairing of 15q11–q13 to the 3′ region of the *GABRB3* gene. The *GABA$_A$R* subunit genes, which encode for subunits of the receptor for the neurotransmitter GABA, are important autism candidate genes (30). Interestingly, while *GABA$_A$R* subunit genes are biallelically expressed in normal brain samples, at least one of these transcripts showed a gain of monoallelic or biased expression in half (4/8) of brain samples from autistic individuals, suggesting underlying epigenetic dysregulation (41). The pairing region likely contains some key regulatory elements for homologous pairing of 15q11–q13 which epigenetically control gene expression in the region. Our analyses revealed discrete MeCP2 and CTCF neuronal-binding sites within the *GABRB3* pairing region were observed in this minimal homologous pairing region required for optimal 15q11–q13 pairing. Differentiated SH-SY5Y cells showed dynamic changes in chromatin structure compared with undifferentiated cells, consistent with a model of active pairing and increased transcription of *GABRB3* with differentiation. Interestingly, previous linkage analyses have shown a significant association between *GABRB3* polymorphisms and autism (42,43). One such *GABRB3* microsatellite has been localized to ~60 kb beyond the 3′ end of the *GABRB3* gene (44) that lies within the *GABRB3* minimal pairing region and interacts with the maternal PWS-IC (Supplementary Material, Fig. S6). Interestingly, maternal transmission of a rare GABRB3 signal peptide variant has been recently observed in autism (45).

Recent findings showed that CTCF and OCT4 together can mediate X-chromosome pairing, and the results of our homologous pairing analyses also suggest that CTCF can mediate specific inter-chromosomal associations in the 3′ region of the *GABRB3* gene (34). Indeed, we identified three potential CTCF-binding sites bordering the homologous pairing region. On the basis of our RNAi-mediated knockdown studies, we conclude that CTCF controls not only X chromosome pairing but also autosomal 15q11–q13 pairing. Although our study highlights CTCF as a central molecule in inter-chromosomal association, its exact role in the etiology of neurodevelopmental disorders remains uncertain. One recent study revealed that CTCF and cohesin complexes are necessary for establishing the chromatin structure required for brain-derived neurotrophic factor transcription (46). Thus, there is already some evidence indicating how epigenetic factors such as CTCF and MeCP2 may play a role in complex psychiatric and neurodevelopmental disorders (16).

It is plausible that MeCP2, such as CTCF, also controls the homologous pairing of 15q11–q13. Mutations in *MECP2* cause RTT, a neurodevelopmental disorder characterized by the loss of speech and acquired motor skills, stereotypical hand movements, and seizures during early childhood (47). In addition, *MECP2* mutations have been found in a few patients diagnosed with AS and autism, suggesting overlap in the pathogenesis of these distinct genetic syndromes (48,49). Consistent with phenotypic and genetic overlap among RTT, AS and autism patients, one previous study demonstrated significant defects in the expression of *UBE3A* and *GABRB3* in brain samples from RTT, AS and autism patients (50). Consistent with results of a previous study utilizing an oligonucleotide decoy approach, we demonstrated that homologous pairing at the *GABRB3* locus was significantly impacted by siRNA-mediated MeCP2 knockdown (20). This finding suggests that inter-chromosomal associations such as homologous pairing are essential for precise gene expression of *GABRB3* during neuronal differentiation. Further experiments are needed to determine how homologous pairing controls the expression of *GABRB3* transcripts. In a simple model, homologous 15q11–q13 pairing might provide a transcriptionally positive environment by recruiting homologous alleles at the same transcription factory to increase neuronal gene expression by recycling positive factors at both alleles. Indeed, the transcriptional inhibitor α-amanitin caused a significant decrease in the homologous 15q11–q13 pairing, further demonstrating the requirement of active transcription for homologous 15q11–q13 pairing.

Recently, development of new techniques such as the chromosomal conformation capture (3C) assay has enabled description of long-range intra-chromosomal associations, such as those at the *H19-Igf2* and *Dlx5/Dlx6* loci (51,52). Similar intra-chromosomal associations have been proposed in the regulation of 15q11–q13 genes because PWS-IC acts in *cis* to regulate paternal expression of *MKRN3*, *MAGEL2*, *NDN* and *SNRPN* genes within 15q11–q13 (53). In support of this hypothesis, our DNA-RNA FISH results showed that the PWS-IC makes an allele-specific association with the homologous pairing region of the *GABRB3* locus in differentiated SH-SY5Y cells (Supplementary Material, Fig. S6). These results may indicate that the intra-chromosomal association between the PWS-IC and *GABRB3* occurs on the maternal 15q11–q13 allele. On the other hand, disassociation of the PWS-IC and *GABRB3* is consistent with paternal allele-specific decondensation of chromatin at this locus during neuronal maturation (54). We speculate that maternal 15q duplication might alter the intrachromosomal association between the PWS-IC and *GABRB3*, thus disrupting the coordinated gene regulation of 15q11–q13.

In conclusion, 15q11–q13 appears to be a useful model region for studying epigenetic pathways and mechanisms such as long-range chromatin organization and homologous pairing. Our observations imply that CNVs such as 15q duplication alter such epigenetic mechanisms, thus disrupting regulation of individual genes at the level of inter- and intra-chromosomal associations. In order to fully understand how CNVs affect the nucleus on a molecular level, it will be important to define chromosomal regulatory elements using diverse genetic approaches, such as MMCT. Furthermore, the characterization of MeCP2 as well as CTCF can reveal additional partners involved in regulation of inter- or intra-chromosomal associations. The investigation of such interplaying partners will help in designing potential drug targets, enabling the development of a therapeutic approach for the treatment of dup15q syndrome.

MATERIALS AND METHODS

Cell lines

A9 hybrids containing a maternal human chromosome 15 tagged with pST*neo* were constructed as previously described (55) and were cultured in Dulbecco's modified Eagle medium (DMEM) (WAKO, Tokyo, Japan) supplemented with 10% calf serum (Hyclone, Thermo Scientific, Waltham, MA,

USA) and 800 μg/ml G418 (Nakarai, Kyoto, Japan). SH-SY5Y neuroblastoma cells (ATCC, USA) were cultured in the DMEM/F12 medium (WAKO) supplemented with 15% fetal bovine serum (Hyclone, Thermo Scientific). For FISH analysis, cells were seeded onto Lab-Tek™ II-CC2™ Chamber Slides (Nalge Nunc, Penfield, NY, USA) and grown until they reached 30–50% confluency. Cells were fixed either before (untreated) or 72 h after the addition of 16 nM PMA (PMA treated) for 15 min in Histochoice (Amresco, Solon, OH, USA) and then washed in 1× PBS/0.5% Tween 20 for 5 min and stored in 70% ethanol at −20°C. For α-amanitin experiments, PMA-treated SH-SY5Y cells were treated with 20 or 30 μg/ml α-amanitin for 4 h.

Microcell-mediated chromosome transfer

Introduction of an extra maternal human chromosome 15 into human SH-SY5Y neuronal cells was performed via MMCT, as previously described (56). Briefly, microcells purified from 1×10^8 donor A9 cells containing a maternal human chromosome 15 were fused with SH-SY5Y cells using 47% polyethylene glycol 1000 (PEG1000: Mr 1000; Nakarai). SH-SY5Y microcell hybrid clones were selected individually in the DMEM/F12 medium supplemented with 15% FBS and 600 μg/ml of G418 for 2–3 weeks. These clones were usually maintained stably in culture under appropriate selective conditions. The introduction of maternal human chromosome 15 in SH-SY5Y cells was confirmed by PCR-RFLP analysis and cytogenetic analysis. The primers for RFLP analysis were 5′-AGTGGGCTTCCCTC-ACTTCT-3′ (forward) and 5′-CAGACAGGCTCCACTTAC-CC-3′ (reverse). Three independent SH-SY5Y cells with an extra maternal human chromosome 15 obtained from each chromosome transfer were selected for further expression and pairing analyses.

Cytogenetic analysis

To confirm the presence of the transferred human chromosome 15 in SH-SY5Y cells, FISH analysis was performed on fixed metaphase spreads of each SH-SY5Y clone using the Vysis LSI Prader-Willi/Angelman Region Probe (GABRB3) (Abbott, North Chicago, IL, USA), as described previously (21). Chromosomes were counterstained with DAPI (Sigma, St Louis, MO, USA).

FISH and pairing assays

DNA FISH analysis was performed as described previously (54). Briefly, FISH was conducted in SH-SY5Y neuroblasts and SH-SY5Y neurons differentiated by 72 h treatment with 16 nM PMA (20). FISH probes for *GABRB3* and *CEP15* were obtained commercially from Vysis, but to determine precise locations of pairing, BAC probes were obtained (CHORI, Oakland, CA, USA). BAC DNA was labeled with Green-dUTP or Orange-dUTP (Abbott). BAC clones for FISH are as follow; RP11-69H14 (*CYFIP1*), RP11-373J1 (*NDN*), RP11-125E1 (*SNRPN*), RP11-171C8 (*HBII-85*), RP11-1081A4 (*UBE3A*), RP11-339C21 (*ATP10A*), RP11-92F7 (*TJP1*), RP11-714E8 (*CHRNA7*), RP11-638J6 (*GABRB3*(1)), RP11-345N11 (*GABRB3*(2)), RP11-974L14 (*GABRB3*(3)), RP11-243J20 (*GABRA5*), RP11-89E18 (*GABRG3*), RP11-79M7 (*GABRG1*), RP11-905L4 (*GABRA2*), RP11-620L1 (*GABRA4*), RP11-1059P8 (*GABRB1*), RP11-315P17 (*GABRB2*(1)), RP11-833C4 (*GABRB2*(2)), RP11-348M17 (*GABRA1*), RP11-204E3 (*GABRG2*), RP23-24D4 (*Gabrb3*, I), RP23-143O21 (*Gabrb3*, II) and RP23-459J11 (*Gabrb3*, III). A nick translation kit (Roche, Penzberg, Germany) was used to create probes, which were then hybridized to cells fixed in Histochoice (Amresco), then dehydrated in 70, 90 and 100% ethanol (10 min each) and dried at 50°C. FISH probes were denatured with the fixed cells at 80°C for 2 min and then hybridized overnight at 37°C on cover-slipped slides. Cells were washed three times in 50% formamide/50% 2× SSC for 5 min, 2× SSC for 5 min and 2× SSC/0.1% IGEPAL for 5 min at 46°C and then mounted in Vectashield (Vector Laboratories, Burlingame, CA, USA) containing 5 μg/μl DAPI. To analyze pairing, we took digital images with a BX51 fluorescence microscope (Olympus, Tokyo, Japan) equipped with a RETIGA EXi CCD camera (Qimaging, Surrey, Canada); these were processed in iVision 4.0 software (BioVision Technologies, Exton, PA, USA). The iVision software was also used to measure distances between two signals. All FISH distances are measured in 2D in this study because 3D is less of a concern for neurons, which are relatively flat compared with round nuclei seen in lymphocytes. Although 2D may change some measurements, signals that are significantly closer than expected of random were likely to be close in 3D space. To simplify the analysis of homologous association or 'pairing' as has been described previously (19,20), nuclei with FISH signals ≤ 2 μm apart were scored as 'paired', while nuclei with two FISH signals >2 μm apart were scored as 'unpaired'. In case of SH(15M) cells, we measured the shortest inter-chromosomal distances between the three signals. Measurement and scoring of FISH signals were performed manually and results are averages of at least three independent scores per sample.

Gene expression analysis

Total RNA was extracted using RNeasy columns, according to the manufacturer's protocols (Qiagen, Hilden, Germany) and then treated with RNase-free DNase I (Takara, Kyoto, Japan). First-strand cDNA synthesis was carried out with random primers and SuperScript® III reverse transcriptase (Invitrogen, Carlsbad, CA, USA). Quantitative RT–PCR was performed with GoTaq® qPCR Master Mix (Promega, Fitchburg, WI, USA) on a CFX384 Real-Time PCR Detection System (Bio-Rad, Hercules, CA, USA). Three replicate reactions were conducted for each gene analyzed. Melting curve analysis was performed to ensure that a single product was amplified with each primer set. Relative expression levels of 15q11–q13 transcripts were normalized by using the comparative Ct (ΔΔCt) method and the geometric average of a set of two housekeeping genes (*GAPDH* and *ACTB*) by the Bio-Rad CFX manager software (version 1.5). Primer sequences are available on request.

RNAi knockdown

We carried out siRNA-mediated knockdown of MeCP2, CTCF and RAD21 proteins using Accell SMART pool siRNAs,